

1
2
3
4
5
6
7
8
9
10
11
12
13
14
15
16

New particle formation in the Svalbard region 2006 - 2015

Jost Heintzenberg¹, Peter Tunved², Martí Galí³, and Caroline Leck⁴

1: Leibniz Institute for Tropospheric Research (TROPOS), Permoserstr. 15, 04318 Leipzig, Germany

2: Department of Environmental Science and Analytical Chemistry (ACES), Stockholm University, 10691 Stockholm, Sweden

3: Takuvik Joint International Laboratory & Québec-Océan, Université Laval, G1V 0A6 Québec, Canada

4: Department of Meteorology, Stockholm University (MISU), 10691 Stockholm, Sweden

rev. 2017-2-18 10:48
Gelöscht: Applied

rev. 2017-2-18 10:48
Gelöscht: ,

rev. 2017-2-18 10:48
Gelöscht: (MISU),

20 Abstract

21

22 Events of new particle formation, (NPF), were analyzed in a ten-year data set of hourly
23 particle size distributions recorded on Mt. Zeppelin, Spitsbergen, Svalbard. Three different
24 types of NPF-events were identified through objective search algorithms. The first and
25 simplest algorithm utilizes short-term increases in particle concentrations below 25 nm,
26 (PCT-events). The second one builds on the growth of the sub-50 nm diameter-median,
27 (DGR-events), and is most closely related to the classical “banana-type” of events. The third
28 and most complex, so-called multiple-size approach to identifying NPF-events builds on a
29 hypothesis suggesting the concurrent production of polymer gel particles at several sizes
30 below about 60 nm, (MEV-events).

31 As a first and general conclusion we can state that NPF-events are a summer phenomenon
32 and not related to Arctic haze, which is a late winter-to-early spring feature. The occurrence
33 of NPF-events appears to be somewhat sensitive to the available data on precipitation. The
34 seasonal distribution of solar flux suggests some photochemical control that may affect
35 marine biological processes generating particle precursors and/or atmospheric photochemical
36 processes that generate condensable vapors from precursor gases. Notable, the seasonal
37 distribution of the biogenic methanesulfonate, (MSA), follows that of the solar flux although
38 it peaks before the maxima in NPF-occurrence.

39 A host of ancillary data and findings point to varying and rather complex marine biological
40 source processes. The potential source regions for all types of new particle formation appear
41 to be restricted to the marginal ice and open water areas between Northeastern Greenland and
42 Eastern Svalbard. Depending on conditions yet to be clarified new particle formation may
43 become visible as short bursts of particles around 20 nm, (PCT-events), longer events
44 involving condensation growth, (DGR-events), or extended events with elevated
45 concentrations of particles at several sizes below 100 nm, (MEV-events). The seasonal

rev. 2017-2-18 10:48

Gelöscht: event.

rev. 2017-2-18 10:48

Gelöscht: appear

rev. 2017-2-18 10:48

Gelöscht: Whereas

49 distribution of NPF-events peaks later than that of MSA and, DGR and in particular of MEV-
50 events reach into late summer and early fall with much open, warm, and biologically active
51 waters around Svalbard. Consequently, a simple model to describe the seasonal distribution
52 of the total number of NPF-events can be based on solar flux, and sea surface temperature,
53 representing environmental conditions for marine biological activity, and condensation sink,
54 controlling the balance between new particle nucleation and their condensational growth.
55 Based on the sparse knowledge about the seasonal cycle of gel-forming marine
56 microorganisms and their controlling factors we hypothesize that the seasonal distribution of
57 DGR and more so MEV-events reflect the seasonal cycle of the gel-forming phytoplankton.

58

59

60 1. Introduction

61

62 In the late 1970ies and early 1980ies the interest in the Arctic atmospheric aerosol widened
63 from the well-identified winter phenomenon of Arctic haze (Rahn and Shaw, 1977;
64 Heintzenberg and Leck, 1994) to summer conditions in this northernmost remote region. In
65 the pristine Arctic summer air the so-called background aerosol (Junge, 1963) was expected
66 to be most clearly visible, far away from the northern hemispheric anthropogenic emission
67 centers at lower latitudes. Episodic and localized occurrences of high concentrations of
68 ultrafine particles, (here defined as particles with diameters < 100 nm), in the summer Arctic
69 were explained by rare import of polluted air from lower latitudes (Flyger and Heidam, 1978;
70 Heintzenberg and Larssen, 1983) or hypothetical anthropogenic sources in the Arctic
71 (Jaenicke and Schütz, 1982).

72 With the advent of sensitive condensation nuclei counters (Agarwal and Sem, 1980) and
73 differential mobility analyzers (Knutson and Whitby, 1975b, a), more details became visible in
74 the Arctic sub-micrometer aerosol. High numbers of ultrafine particles were observed in
75 connection with fog passages (Lannefors et al., 1983) and chemical aerosol information
76 indicated a regional – possibly biogenic – particle sources in the summer Arctic
77 (Heintzenberg, 1989). The high molar ratios of methane sulfonate, (MSA), to non-sea salt
78 sulfate, (nssSO_4^{2-}), of 0.28 in the Arctic summer aerosol found by Heintzenberg and Leck
79 (1994) substantiated the biogenic source of the particles.

80 The establishment of long-term Arctic aerosol monitoring at the fringes of the pack ice in
81 Alaska (e.g., Polissar et al., 1999), Canada (e.g., Norman et al., 1999; Willis et al., 2016), and
82 on Spitsbergen (e.g., Tunved et al., 2013), revealed more details of potential sources of the
83 summer aerosol, in particular their connection to the marine biosphere in the Arctic. The
84 unique series of systematic aerosol studies in the central Arctic north of 80°N onboard the
85 Swedish icebreaker *Oden* in 1996 led to the formulation of a new hypothesis concerning a

rev. 2017-2-18 10:48

Gelöscht: (Knutson and Whitby, 1975a, b)

rev. 2017-2-18 10:48

Gelöscht: (e.g., Tunved et al., 2013)

88 specific process of marine biogenic particle formation (Leck and Bigg, 1999). The marine
89 biogenic particles involved behaved as polymer gels and originated in the surface microlayer
90 (SML) of the ocean, (Orellana et al., 2011b), from the activity of sea-ice algae,
91 phytoplankton and, perhaps, bacteria. The new particle events were reported to occur as
92 simultaneous enhancement of particle number concentrations in the whole size-range below
93 50 nm, and not with the prototypical “banana growth” (Kulmala et al., 2004). Two more
94 *Oden* cruises in 2001 and 2008 yielded results that were partly contradicting (Held et al.,
95 2011b; Held et al., 2011a), partly supporting the SML hypothesis (Leck et al., 2013; Karl et
96 al., 2013; Orellana et al., 2011b; Leck and Bigg, 2010). The synopsis of the results of four
97 *Oden* cruises of Heintzenberg et al. (2015) identified geographic regions of new particle
98 formation (NPF) in the inner Arctic while stressing the importance of recent open water and
99 related biological activity in the sea in transects by air masses with new particle formation
100 over the central Arctic.

101 Two years of aerosol size distributions from Mt. Zeppelin, Spitsbergen and Alert, both
102 located at the fringes of the central pack ice, were analyzed by Croft et al. (2016a) with a
103 global aerosol geophysics model. They discuss classical new-particle nucleation, coagulation
104 scavenging in clouds, scavenging by precipitation, and transport in order to explain the annual
105 cycle of the Arctic aerosol. Croft et al. (2016a) find two seasonal maxima in their modeled
106 particle nucleation rates, one in March, and one in July. In spring, their simulated NPF occurs
107 mainly in the free troposphere, whereas in summer, it occurs also in the planetary boundary
108 layer. More recently, Croft et al. (2016b) state that ammonia from seabird-colony guano is a
109 key factor contributing to bursts of newly formed particles, which are observed every summer
110 in the near-surface atmosphere, at least at Alert, Nunavut, Canada. Earlier, the results of
111 studies with another global aerosol model by Browse et al. (2014) suggested that the potential
112 increase in NPF in the Arctic with potential increases in cloud condensation nuclei is

113 compensated by wet scavenging. They also state that scavenging by pre-existing large
114 particles suppresses NPF-events.

115 Based on three years of data from the two Arctic sites Thule and Ny-Ålesund (gruvebadet)
116 Becagli et al. (2016) examined the sources and environmental factors controlling the
117 biological aerosol component MSA. Their analysis included satellite-derived Chlorophyll-*a*
118 (an indicator of phytoplankton biomass), oceanic phytoplankton primary productivity, (PPP),
119 and sea ice. Whereas they found good correlations between MSA, PPP and sea ice, (the latter
120 two being closely related), their data did not allow any statements on NPF processes.

121 To date the longest record of sub-micrometer number-size distributions of the Arctic
122 aerosol down to 5 nm particle diameter and below has been accumulated on Mt. Zeppelin,
123 Spitsbergen (Tunved et al., 2013; Heintzenberg and Leck, 1994). For the ten years from 2006
124 through 2015 a total of 63936 quality-controlled hours of aerosol data are available, i.e.
125 during 73% of all hours of the ten years. In the present study we exploit this formidable data
126 set in a search for processes forming new particles. An important first step in this work was
127 formulating completely objective criteria for the identification of events. In the relatively
128 clean Arctic environment we do not expect the classical nucleation and growth events as
129 frequently observed over the continents, (cf. Kulmala et al., 2004), to dominate. Thus, we
130 refrained from applying the objective search algorithm formulated by Heintzenberg et al.,
131 (2007) for this “Banana-type” of events. Instead we formulated new objective search
132 algorithms allowing several potential types of new particle formation events or formation
133 processes. With a host of complementary atmospheric and surface physical, chemical, and
134 biological information a large number of NPF-events identified with these algorithms will be
135 analyzed in the following chapters.

136

137

138

139 **2. Database**

140

141 The Mt. Zeppelin observatory

142

143 Situated at the top of Mt Zeppelin, Svalbard (78° 56'N, 11° 53'E), the Zeppelin observatory
144 offers a unique possibility to study the characteristic features of Arctic atmospheric
145 constituents such as trace gases and aerosol particles. At a height of 474 m a.s.l. the station is
146 located near the top of the local planetary boundary layer and represents remote Arctic
147 conditions. The closest source of pollution, the small community of Ny-Ålesund, is located
148 ~2 km north of the station
149 (http://www.esrl.noaa.gov/psd/iasoa/sites/default/files/stations/nyalesund/nyalesund_site.jpg).

150 However, the elevation difference and typical wind patterns largely prevent pollution from
151 nearby sources to reach the Zeppelin Observatory. The dominating wind pattern is east-
152 southeast katabatic flow from Kongsvegen glacier or from northwesterly directions as
153 channeled by the Kongsfjord (Beine et al., 2001; Heintzenberg et al., 1983). The station itself
154 was initially established in 1991, and is owned by the Norwegian Polar Research Institute
155 (NP). The Norwegian Institute for Air Research (NILU) is responsible for the coordination of
156 the scientific program.

157

158

159 **2.1 Physical aerosol data**

160

161 After a period of continuous aerosol measurements by the Department of Meteorology,
162 Stockholm University in the early 1990ties, (Heintzenberg and Leck, 1994), the Department
163 of Analytical Chemistry and Environmental Science, Stockholm University, initialized
164 observations of the aerosol number size distribution in mid-2000. Originally, the system

165 consisted of a single differential mobility analyzer system, (DMPS), consisting of a medium-
166 size Hauke-type differential mobility analyzer, (DMA), together with a TSI 3760
167 condensation particle counter, covering diameters between 20 and ~500nm. From 2006 on
168 the particle size range was widened covering particle sizes between 10 and 790 nm. In 2005,
169 the rain-cover over the inlet was replaced. Initially, the instrument inlet was of a PM10 type,
170 removing particles or hydrometeors with diameters $>10\ \mu\text{m}$ from the sampled air stream.
171 During a substantial renewal of the Stockholm University equipment in 2010-2011, both inlet
172 and DMPS system were replaced.

173 Since then, the DMPS-system utilizes a custom-built twin DMA-setup comprising one
174 Vienna-type medium DMA coupled to a TSI CPC 3010 covering sizes between 25-800 nm
175 and a Vienna-type long DMA coupled with at TSI CPC 3772 covering sizes between 5-60
176 nm. The size distributions from the two systems are harmonized on a common size grid and
177 then merged. Both systems use a closed-loop flow setup. The current inlet hat is of whole air
178 type, complying with EUSAAR¹ standard for high altitude or Arctic sampling conditions. In
179 the current setup, the inlet is operated with a flow of ca. 100 liters per minute, (lpm). Laminar
180 flow conditions apply throughout the sampling lines. Outside of the station, the inlet
181 temperature is kept above 0°C using active heating. Inside the station the temperature
182 increases gradually to room temperature (maximum temperature reaches ca. 25 °C, but
183 remains typically around 20°C). Relative humidity, (RH) and temperature are internally
184 monitored and measurements are maintained at dry conditions with $\text{RH} < 30\%$. The system is
185 regularly checked with latex spheres and flow controls. The recorded data are manually
186 screened and crosschecked with other available observation as in Tunved et al. (2013). If
187 inconsistencies were found between the different datasets, further investigation was

¹ EUSAAR (European Supersites for Atmospheric Aerosol Research) is an EU-funded I3 (Integrated Infrastructures Initiatives) project carried out in the FP6 framework of the specific research and technological development gram "Structuring the European Research Area - Support for Research Infrastructures", (<http://www.eusaar.net/>).

rev. 2017-2-18 10:48

Gelöscht: (2013).

189 performed to exclude data that were identified as affected by instrumental errors. Using the
190 instrumental logbook, periods of local activity potentially influencing the sampling were also
191 excluded from the dataset. During the years 2006 – 2010 no particles below ten nanometers
192 in diameter were recorded. From 2011 on four more diameter bins down to 5 nm were
193 included and a different diameter array was utilized. To allow for a synopsis of all years all
194 size distributions were interpolated on the pre-2011 diameter array and all integrals of the size
195 distribution over particle diameter were taken over the joint diameter range 10 to 631 nm. For
196 the pre-2011 years the data at the four size channels below 10 nm were flagged as missing.
197 However, whenever results cover the complete time series the resulting number
198 concentrations in the four first channels covering the years 2011 – 2015 are carried along.

199 For the identification of NPF in terms of particle growth the parameter D50 in nanometer
200 was calculated as the number median diameter of particles smaller than 50 nm but larger than
201 10 nm, i.e. 50% of all particles below that size are smaller than D50. Besides this parameter
202 Table 1 lists nine integral particle parameters, which are utilized in the NPF-search
203 approaches or in the interpretation of results. These aerosol parameters quantify total particle
204 number, (NTO), and particle numbers in sub-ranges of the number size distribution such as
205 N25, quantifying the total number of particles between ten and 25 nm.

206 Following the concept developed by Pirjola et al., (1999), and Kulmala et al., (2001) we
207 calculated the condensation sink, (CS, s^{-1}), as a parameter with which the probability of new
208 particle formation from the gas phase and the necessary amount of condensable vapor can be
209 estimated. We utilized number size distributions, pressure and temperature taken from our
210 database for this calculation.

211
212
213
214

rev. 2017-2-18 10:48

Gelöscht: For this calculation we

rev. 2017-2-18 10:48

Gelöscht: from our database

217 2.2 Chemical aerosol data

218

219 For the interpretation of NPF-events we employed chemical information derived from the
220 analyses of high volume particle samples taken by the Norwegian Institute for Air research,
221 (NILU). A high volume sampler (PM10) was used to collect samples for a quantitative
222 determination of sodium, (Na^+), sulfate, (SO_4^{2-}) and MSA (CH_3SOO^-). The sampler collected
223 material for analysis in one to three days. Blank samples were obtained by mounting the
224 glass fiber filters at the sampling site with the same sampling period but without air passing
225 through. Na^+ and SO_4^{2-} were analyzed by NILU and have been downloaded for the present
226 study from the EBAS database (<http://ebas.nilu.no>), which list details about the sampling
227 technique and the sampling protocol. ~~Nss SO_4^{2-} was determined from total sulfate correcting~~
228 ~~for sea salt sulfate, as $0.25 \times \text{Na}^+$~~ (Keene et al., 1986).

229 MSA was analyzed at the laboratory of the Department of Meteorology, Stockholm
230 University. To allow for subsequent chemical determinations the ambient samples and blanks
231 were carefully handled in a glove box (free from particles, sulfur dioxide and ammonia). At
232 the time of the chemical analyses, still in the glove box, the substrates were extracted (in
233 centrifuge tubes) with 60 cm³ deionized water (Millipore Alpha-Q, conductivity 18 MΩcm).
234 The extracts were thereafter analyzed for weak anions by chemically suppressed ion
235 chromatography (IC, Dionex ICS-2000) using Dionex AG11/AS11 columns. In order to trap
236 carbonates and other ionic contaminants a Dionex ATC-1 column was used before the
237 injection valve. The injection volume was 50 μdm³. Quality checks of the IC-analyses were
238 performed with both internal and external reference samples (Das et al., 2011). The analytical
239 detection limits obtained for the various ions, defined as twice the level of peak-to-peak
240 instrument noise, was 0.0001 μeq dm⁻³ for MSA. The overall analytical accuracy was better
241 than 1.5%.

242

rev. 2017-2-18 10:48

Gelösch: *)

rev. 2017-2-18 10:48

Gelösch: To be able to apportion the measured

rev. 2017-2-18 10:48

Gelösch: to nss SO_4^{2-} the observed concentrations of Na^+ were used

rev. 2017-2-18 10:48

Gelösch: the reference element based on the assuming that all Na^+ is of marine origin,

250 **2.3 Back-trajectories and meteorological data**

251

252 For every hour during the ten years 2006 through 2015 three-dimensional back trajectories
253 have been calculated arriving at 474 m at Mt. Zeppelin. The trajectories have been calculated
254 backward for up to ten days using the HYSPLIT4 model (Draxler and Rolph, 2003) with
255 meteorological data from the Global Data Assimilation System with one-degree resolution
256 (GDAS1). Trajectories extending backwards for ten days are inaccurate at origin due to the
257 trajectory uncertainty of 25-30% of its length, (Stohl, 1998). More information about the
258 GDAS dataset can be found at Air Resources Laboratory (ARL), NOAA
259 (<http://ready.arl.noaa.gov>), from which the meteorological data were downloaded.

260 During the analyzed time period meteorological records at the Mt. Zeppelin station are
261 rather limited in quality and were frequently interrupted. There are no precipitation
262 measurements and wind measurements are strongly influenced by the station building and by
263 the local topography. In order to have an internally consistent, and unbroken meteorological
264 record we utilized hourly meteorological parameters at trajectory arrival times as calculated
265 by the HYSPLIT4 model. We emphasize that their accuracy depends on the quality of the
266 meteorological model inside HYSPLIT4 and the accuracy and representativeness of the
267 meteorological fields utilized by the model. Of the local meteorological record air
268 temperature was considered the most reliable and thus explored in a comparison of trajectory
269 calculated and modeled meteorological data. When comparing the 42600 contiguous hourly
270 records from 2008-01-01 until 2012-11-10 the average ratio of measured and calculated
271 temperatures is 0.98, with a coefficient of determination of 0.96. The utilized model
272 parameters are listed in Table 1.

273 As an additional parameter we evaluated the vertical air movement of the trajectories
274 during the last hour before arrival by subtracting the trajectory height one hour before arrival

rev. 2017-2-18 10:48

Gelöscht: the

276 at the arrival height of 474 meter. The resulting vertical displacement parameter, DZ, is given
277 in meters per hour. Positive values of DZ indicate a lifting of the air.

278 The most important missing meteorological information concerns the local cloud cover.
279 No direct recording was available of times during which the station was in clouds. The
280 closest available cloud instrument is a ceilometer operated by the Alfred Wegener Institute
281 (AWI) at their Koldewey Station in Ny-Ålesund, i.e. in the valley below Mt. Zeppelin, some
282 2.8 km of horizontal distance from the position of the mountain station. From the one-minute
283 records of the ceilometer we derived hourly values of the 25% percentile of cloud base, which
284 was used as an indicator for the Zeppelin station being in cloud. This ceilometer parameter is
285 listed as C25 in Table 1.

286 Precipitating clouds scavenge the planetary boundary layer and thus reduce the available
287 particle surface as condensation sink of particle precursors. As a consequence nucleation
288 from the gas phase may be facilitated (Tunved et al., 2013). As in Tunved et al. (2013) we
289 utilized the HYSPLIT-modeled precipitation along the back trajectories. Sums of
290 precipitation, (SP, see Table 1), were calculated along each back trajectory and will be
291 referred to as SP1 (during the last day), SP2 (during the last but one day), and SP5 (during
292 days three to five) before arrival at Mt. Zeppelin.

295 2.4 Marine biological data

296
297 The biologically active marginal ice zone is a major natural source of sulfur in the Arctic
298 summer atmosphere, (Leck and Persson, 1996b, a), and Wiedensohler et al. (1996), indicated
299 a potentially important role of dimethyl sulfide (DMS) in regional new particle formation.
300 DMS emissions from the sea have long been proposed to control new particle formation in the
301 marine boundary layer, (Charlson et al., 1987), which builds on DMS_{aq} being transported via

rev. 2017-2-18 10:48

Gelösch: cloudiness

rev. 2017-2-18 10:48

Gelösch: clouds. The meteorological parameters are

rev. 2017-2-18 10:48

Gelösch: . Precipitating clouds scavenge the planetary boundary layer and thus reduce the available particle surface for condensational uptake of particle precursors. As a consequence nucleation from the gas phase may be facilitated (Tunved et al., 2013). As in Tunved et al. (2013) we utilized the HYSPLIT-modeled precipitation along the back trajectories. Sums of precipitation, (SP, see Table 1), were calculated along each back trajectory and will be referred to as SP1 (during the last day), SP2 (during the last but one day), and SP5 (during days three to five) before arrival at Mt. Zeppelin.

319 turbulence and diffusion to the sea-air interface, represented by the transfer velocity, which in
320 turn depends on sea-surface temperature, salinity, and wind speed, (Liss and Merlivat, 1986).

321 | Once in the atmosphere DMS_g is photochemical oxidized via intermediates such as sulfuric
322 acid and methane sulfonic acid, (Ayers et al., 1996), which eventually leads to the formation
323 of aerosol nssSO_4^{2-} and MSA. The products of the photochemical oxidation of DMS the ratio
324 MSA/ nssSO_4^{2-} show a temperature dependence (Bates et al., 1990), favoring MSA in the cold
325 Arctic environment (Karl et al., 2007).

326 Dimethyl sulfide in the ocean (DMS_{aq}) is produced through the degradation of its algal
327 precursor dimethylsulfoniopropionate (DMSP) by microbial food webs, (Simó, 2001). At
328 high latitudes, total DMSP (DMSPt) and therefore DMS_{aq} , essentially follows the seasonal
329 cycle of phytoplankton biomass, (Lana et al., 2012). DMSPt is defined as the sum of
330 $\text{DMSP}_{dissolved}$ and $\text{DMSP}_{particulate}$ concentration. Yet, the amount of DMSPt per unit
331 phytoplankton biomass may vary depending on species composition and physiological state,
332 (Keller et al., 1989).

333 The dissolved organic carbon (DOC) concentrations in surface waters of the high Arctic
334 Ocean are up to ten times higher than in any other ocean basin and closer in range to DOC
335 levels reported for sea ice (Gao et al., 2012). A large fraction of DOC spontaneously
336 assembles into polymer gels: polysaccharide forming hydrated calcium bonded three-
337 dimensional networks to which other organic compounds, such as proteins and lipids, are
338 readily bound. The assembly and dispersion of the polysaccharide molecules can be affected
339 by environmental parameters, such as UV-B radiation (280-320nm) dispersing or inhibiting
340 gel formation, and/or pH and temperature inducing gel volume phase changes (swelling and
341 shrinkage). In the study of Orellana et al., (2011b), the swelling and shrinking of the
342 polysaccharide networks or polymer gels were also causally related by additions of nano to
343 micromolar levels of DMS and DMSP. High DMSP concentrations have also been measured

rev. 2017-2-18 10:48

Gelöscht: ventilated to

345 in the mucilage surrounding prymnesiophyte *Phaeocystis pouchetii* colonies in Arctic waters,
346 representing up to 25% of the total water column DMSP pool, (Matrai and Vernet, 1997).
347 The findings made by Orellana et al., (2011b) were in agreement with previous findings by
348 Orellana et al., (2011a) that high concentrations of DMSP and DMS are stored in the acidic
349 secretory vesicles of the *Phaeocystis* algae where DMSP is trapped within the condensed
350 polyanionic gel matrix until the secretory vesicles are triggered by environmental factors such
351 as temperature to release gels that undergo volume phase transition and expand at the higher
352 pH of seawater. Exocytosis of polymer gels accompanied by elevated DMS and DMSP
353 concentrations suggests the transport of these chemical compounds by the gel matrix.
354 Schoemann et al., (2005) report that *Phaeocystis antarctica* is particularly well adapted to low
355 temperatures, being more competitive than *P. pouchetii* for temperatures between -2 and
356 +2 °C. *Phaeocystis pouchetii*, however, appears to be better adapted to temperatures closer to
357 5 °C. In the Arctic a higher occurrence of the *Phaeocystis pouchetii* would be expected in the
358 northward advection of warm Atlantic water masses around Svalbard.

359 Here we estimated DMSPt at the sea surface using the algorithm described by Galí et al.
360 (2015). The DMSPt algorithm exploits the distinct relationship between DMSPt and
361 Chlorophyll-*a* depending on the light exposure regime of the phytoplankton community. The
362 light exposure regime is defined by the ratio between euphotic layer depth and mixed layer
363 depth (Z_{eu}/MLD). Additional predictor variables used are sea surface temperature (SST) and
364 particulate inorganic carbon (PIC), which is used in the algorithm as a proxy for
365 coccolitophores such as *Emiliana huxleyi*. During late bloom stages, the calcite plates that
366 cover coccolitophore cells (called coccoliths) detach and cause an increase in seawater
367 backscatter that invalidates satellite retrievals of Chlorophyll-*a*. Therefore, inclusion of PIC
368 in the algorithm as a proxy for DMSPt increases data coverage. Although the algorithm was
369 developed for the global ocean, validation results with in situ data indicate that it performs as
370 well or slightly better in Arctic and sub-Arctic waters.

371 The use of remotely sensed DMSPt as a proxy for marine DMS_{aq} emission is a significant
372 improvement with respect to prior studies that used Chlorophyll-*a* (Becagli et al., 2016;
373 Zhang et al., 2015). Yet, it is not ideal because (i) the ratios DMS_{aq}/DMSPt in surface
374 seawater are variable, and tend to be higher in high solar irradiance and nutrient-poor
375 conditions typical of summer, (Gali and Simó, 2015), and (ii) even if DMSPt is a better proxy
376 for DMS_{aq}, the influence of meteorological and sea surface conditions (mainly wind speed
377 and SST) on the sea-air flux of DMS_{aq} is not taken into account. Development is underway of
378 an algorithm for the retrieval of DMS_g concentrations in air and DMS fluxes.

379 The DMSPt algorithm was run for the 2006-2015 period using daily composites of the
380 Moderate Resolution Imaging Spectroradiometer on the Aqua satellite (MODIS-Aqua) at 4.64
381 km resolution (L3BIN, reprocessing R2014.0) downloaded from NASA's Ocean Color
382 website (<http://oceancolor.gsfc.nasa.gov>). The MODIS variables used include Chlorophyll-*a*
383 concentration derived with the GSM algorithm, (Maritorena et al., 2002), PIC, nighttime SST
384 and Z_{eu}. MODIS nighttime SST was complemented with SST from the Advanced Very High
385 Resolution Radiometer (AVHRR, <https://podaac.jpl.nasa.gov/AVHRR-Pathfinder>) to increase
386 data availability. MLD was obtained from the MIMOC climatology, (Schmidtko et al.,
387 2013), which was linearly interpolated from its original 0.5°x0.5° grid at monthly resolution
388 to the MODIS grid at daily resolution.

389 Satellite remote sensing of biological activity in surface waters requires ice-free and at
390 least part of the time cloud-free. The passive sensing methods of MODIS additionally require
391 a minimum of solar illumination of the scenes (i.e., solar zenith angle < 70°; (IOCCG, 2015)).
392 Consequently, the length of the satellite-observable period used to compute DMSPt means
393 shortens from all-year-round at latitudes <45° to approximately six months (the spring-
394 summer semester) at 80°N. In addition, the annual DMSPt map in Fig. 3 excludes all land and
395 ice covered regions. In order to increase data coverage, daily DMSPt composites were binned
396 to five-day periods and a 46.4 km equal-area sinusoidal grid, (10x10 bins of the original pixel

397 size). The average distance between a trajectory point and the closest center of a MODIS
398 pixel is 18 km.

399 Following the same approach as with the ice data average DMSPt from ocean color data,
400 (OC), along each back trajectory were calculated and will be referred to as OC1 (the last day),
401 OC2 (the last but one day), and OC5 (days three to five) before arrival at Mt. Zeppelin. In
402 this procedure missing data were flagged as such, and were not taken into account.

403

404

405 **2.5 Ice data**

406

407 For the interpretation of events of new particle formation observed during the *Oden* cruises
408 information on pack ice extent under the air masses reaching the sampling points proved
409 crucial (Heintzenberg et al., 2015). Another motivation for utilizing ice data in the present
410 study is the fact that the Svalbard region experiences large seasonal changes in pack ice cover
411 which we expect to have strong effects on emissions of particles and their precursor gases.
412 Thus daily ice concentrations were taken from the NSIDC database (<https://nsidc.org/data>).
413 The irregularly shaped data gap around the pole caused by the inclination of satellite orbits
414 and instrument swath was filled with 100% cover. To each hourly position and data of the
415 back trajectories the ice information in the corresponding maps of ice concentrations were
416 added and displayed in Fig. 2. On average the closest pixel in the ice maps was about 12 km
417 off any trajectory point.

418 In the discussion of results we utilize the complement of ice cover, i.e., the amount of open
419 water because the marine biological processes of interest predominantly take place in the
420 open water, (Leck and Persson, 1996a). As integral parameters average open water, (OW),
421 percentages along each back trajectory were calculated and will be referred to as OW1 (the
422 last day), OW2 (the last but one day), and OW5 (days three to five) before arrival at Mt.

423 Zeppelin. The most solid ice cover is seen in an area reaching from Northeastern edge of
424 Greenland via North Pole to Parry Island. A marginal ice zone extends along the east coast of
425 Greenland to Franz-Josef-Land, and the area between Svalbard and the latter island.

426

427

428 **2.6 ERA-Interim data of sea surface temperature**

429

430 Daily Sea Surface Temperature (SST) data for our study period (2006-2015) were
431 downloaded from the website of the European Centre for Medium-Range Weather Forecasts
432 (ECMWF). A description of the global atmospheric reanalysis, (ERA-Interim), has been
433 given by Dee et al. (2011), and a guide to the products and the download procedures can be
434 found at <http://www.ecmwf.int/en/elibrary/8174-era-interim-archive-version-20>. Briefly,
435 ERA-Interim is an assimilating model reanalysis of the global atmosphere and sea-surface
436 physical parameters covering the data-rich period since 1979. SST data were downloaded at a
437 resolution of approximately 0.56° and regridded onto the same 46 km equal-area sinusoidal
438 grid used for DMSP and cloud fraction, (see below). Ice-covered pixels were screened out
439 prior to the back-trajectory analysis. In the Arctic region, ERA-Interim has been shown to be
440 a top performer among a number of atmospheric reanalyses, (Lindsay et al., 2014).

441

442

443 **2.7 MODIS cloud fraction**

444

445 Persistent cloud cover limits PPP in Arctic and Sub-arctic seas, (Bélanger et al., 2013), and,
446 as mentioned above, irradiance at the sea surface, which is largely controlled by cloudiness,
447 influences $\text{DMSP}_{\text{dissolved-to-DMS}_{\text{aq}}}$ conversion. Boundary layer clouds are known to be
448 additional controllers of the surface aerosol (Heintzenberg, 2012). In the summer Arctic low

449 level clouds and fogs are widespread (Warren and Hahn, 2002). Both scavenging and new
450 particle formation have been observed in connection with low clouds and fog passages
451 (Lannefors et al., 1983; Heintzenberg and Leck, 1994; Leck and Bigg, 1999; Heintzenberg et
452 al., 2006; Karl et al., 2013). Beyond the cloud base derived from the ceilometer we have no
453 other in situ local or regional cloud information. Thus, we utilize satellite-derived cloud
454 information.

455 Daily Level-3 global cloud fraction with one-degree resolution was downloaded from
456 NASA website (<http://modis-atmos.gsfc.nasa.gov>, Hubanks et al., 2015) and extracted for our
457 region of interest. Briefly, level 3 images correspond to the aggregation of all level 2 images
458 (1 km resolution) available within the one-degree resolution grid. For a given L2 scene, each
459 pixel is assigned a value of 1 (cloudy) or zero (clear sky), and then the individual scene values
460 are averaged over a 24-hour period. Note that a given pixel can be revisited up to six or seven
461 times in the course of a day at high latitudes. Finally, the daily composites were re-projected
462 to 46.4 km pixels to match the spatial resolution of DMSPt. The average distance between a
463 trajectory point and the closest MODIS pixel was 18 km.

464 The cloud fraction CF as well as other cloud properties from MODIS have been
465 extensively used, for instance to study the global spatial and temporal distribution of clouds
466 over the last decade (e.g., King et al., 2013). Several studies have also successfully
467 performed validation by comparison with in situ data (e.g., An and Wang, 2015) which
468 demonstrated the ability of the MODIS-aqua sensor to retrieve cloud cover.

469 Following the same approach as with the ice data and DMSPt, average cloud fractions,
470 (CF, see Table 1), along each back trajectory were calculated and will be referred to as CF1
471 (the last day), CF2 (the last but one day), and CF5 (days three to five) before arrival at Mt.
472 Zeppelin. Missing data are flagged as was done with DMSPt data.

473

474

475 3. Three approaches to identifying events of new particle formation

476

477 There are no definitive and no generally accepted methods to identify or predict NPF-events
478 in atmospheric time series of aerosol data. Thus, in the present study we explored different
479 approaches with varying degrees of complexity to identify such events. We emphasize that
480 none of these approaches explicitly is connected to diel cycles such as in Dal Maso et al.,
481 (2005) or makes any assumptions about the time of day during which new particle formation
482 occurs. Three objective search algorithms were written in FORTRAN to analyze the time
483 series of hourly records of aerosol parameters in search of new particle formation:

484 1. The simplest approach of upper percentiles (PCT-approach), assumes that NPF-events are
485 characterized by extremely high concentrations of small particles in terms of N25 (see
486 Table 1). The key parameter characterizing each PCT-event was the value of N25
487 averaged over a fixed number of hours, ($N25_{av}$), after the nominal start of an event, (see
488 below). With $N25_{av}$ also a nominal length of PCT-events was defined as the number of
489 hours after the start of an event by which N25 sank to less than half of $N25_{av}$.

490 2. The more specific approach of diameter growth (DGR-approach) builds on the temporal
491 development of the particle size distribution in terms of a systematic growth of the
492 diameter D50 (see section 4.1) to find the classical “Banana Type” of NPF-event,
493 (Kulmala et al., 2004). The key parameter characterizing each DGR-event was the average
494 growth of D50 during the nominal event length NUC, (see below). For this approach the
495 nominal length of events was reached when the running two-hour average growth fell
496 below the value one.

497 2. The most complex approach of multiple-size events, (MEV-approach), searches for events
498 with concurrent appearance of concentration increases in several size classes below 60 nm
499 diameter (Karl et al., 2013; Leck and Bigg, 2010). The key parameter characterizing each
500 MEV-event was the relative concentration increase averaged over the chosen size classes

501 below 60 nm during the nominal event length NUC, (see below). As with PCT-events a
502 nominal length of MEV-events was defined as the number of hours after the start of an
503 event by which N25 sank to less than half of N25_{av}.

504

505 Three time-related parameters were commonly defined for all three approaches:

506 1. Nominal NPF-event length, (NUC) was nine hours.

507 2. Pre-event periods, (PRENUC), from which increases in diameters or number
508 concentrations were calculated, were six hours.

509 3. Reference periods, (REF), before PRENUC and after NUC periods were defined in order
510 to compare event and pre-event data with non-event conditions. Each of these reference
511 periods had the length of half the sum of pre-event plus event time periods, making the
512 total reference time period of each event as long as that of the event itself.

513 Besides these common characteristic lengths individual fixed thresholds were chosen and
514 discussed below for each approach in order to generate at least 200 unique events per
515 approach, (see Table 2).

516 The aerosol data used to define the NPF-events were complemented by a large number of
517 environmental parameters. The primary temporal resolution of the environmental parameters
518 was between one minute (C25, cf. Table 1) and five days (DMSPt, cf. Table 1). C25 was
519 calculated as 25% percentile on an hourly basis. The parameters with resolutions higher than
520 an hour (OW, CF, and OC, cf. Table 1) were evaluated along the hourly back trajectories.
521 While this procedure yielded hourly varying results even of OW, CF, and OC it has to be kept
522 in mind that this hourly variability is the result of hourly resolved trajectories traversing the
523 grid; the low primary temporal resolutions of the OW, CF, OC, and chemical parameters
524 remain. For these slowly varying parameters the REF periods before and after the events
525 were extended to one day beyond the longest primary resolution, i.e., six days.

526 For two reasons the three search algorithms may yield temporarily redundant results, i.e.,
527 they may identify the same events. One, they go independently through the same time series
528 of aerosol data, possibly causing inter-approach redundancy. Two, each algorithm goes
529 through the time series hour by hour, thus allowing for temporal overlap of events found by
530 each approach, (intra-approach redundancy).

531 The three types of events were assumed to be mutually exclusive and potentially being
532 caused by different sets of conditions for new particle formation. Thus, a FORTRAN
533 procedure was developed to eliminate both intra and inter-approach redundancy while
534 maintaining a maximum of identified NPF-events. To remove intra-approach redundancy the
535 procedure identifies overlapping events within each approach. Of each ensemble of such
536 overlapping events the one with the strongest key parameter of the respective approach
537 (growth of D50, or concentration increases as defined above) is retained. Next, inter-
538 approach redundancy is addressed by the procedure. However, there is no unique solution to
539 the problem of the partly redundant three time series of events. In order to avoid any
540 preference of one or several types of events in the tests of inter-approach overlap pairs of
541 events of different approaches are chosen at random and compared for overlap. This random
542 comparison is done as often as the product of the number of events of the three approaches.
543 This rather time-consuming random test yields stable numbers of non-overlapping events
544 within less than one percent, irrespective of the order in which the events of the three
545 approaches were arranged for the test. By removing intra and inter-approach redundancy in
546 the first two steps of the procedure a number of time periods will be “freed”. Consequently,
547 in a last step, the procedure tries to fill the “freed time periods” non-redundantly with events
548 of the three approaches that had been eliminated in the first two steps. Table 2 collects total
549 numbers and unique numbers of events for each approach. In the rest of the paper only non-
550 redundant events will be discussed. The total number of new particle formation events will
551 be shortened to TNPF.

rev. 2017-2-18 10:48

Gelöscht: -

... [1]

554 3.1 The upper percentile of N25 (PCT-approach)

555

556 Events of new particle formation were identified by time periods in which N25 was
557 consistently, i.e. on average for three hours, above a set threshold. With a threshold of the
558 93%-percentile (170 cm^{-3}) 4143 PCT-events were identified in the total data set, only 240 of
559 which were unique because most of them overlapped with event or pre-event times of the
560 other two approaches. Average N25 during these unique events was 330 cm^{-3} and the average
561 length of events $4 \pm 0.9 \text{ h}$, (one standard deviation).

562 Fig. 4, (top), shows the average temporal development of the relative size distributions for
563 the unique PCT-events as in the results in Karl et al. (2013), i.e. relative concentrations were
564 formed by dividing the absolute number concentrations by the average total number during
565 the six-hour pre-event time periods. The events are characterized by a nearly monomodal
566 distribution around 20 nm that broadens somewhat around the nominal start of the events.
567 During the last three hours before the events D50 decreased slightly and returned to the pre-
568 event level during the nine NUC hours.

569 In connection with PCT-events average aerosol parameters NTO through N300 showed an
570 average increase by a factor of 2.2 during PRENUC-periods, which was maintained on an
571 average level of 1.5 during the events. The aerosol-chemical parameters Na^+ , nssSO_4^{-2} , and
572 MSA were on an average level of 20% of their reference value. The average environmental
573 parameters indicate a strong increase by a factor of 14 in solar radiation and a lifting of cloud
574 base before the events. During the events the level of solar radiation was still elevated by a
575 factor of six above its reference value. As a consequence temperature at the station was up by
576 2 – 3 degrees. Precipitation 12 h before trajectory arrival time, (SP12) was a factor of five
577 above reference levels for air arriving during NUC-periods, whereas SP35 to SP5D were
578 below their respective reference levels. Cloud fractions were slightly raised 12 - 48 h before
579 air arrival. Of the ocean parameters more open water was met by trajectories 12 to 24 before

580 their arrival with ocean temperatures 12 to 48 h before trajectory arrival having been up to
581 four degrees warmer than their respective reference values. On average DMSPt-parameters
582 OC24 through OC5D showed were raised by a factor of two above their reference value.

583 In Fig. 5, (left top panel), average trajectory height profiles during PRENUC and NUC-
584 periods are displayed. Widely varying vertical air mass paths occurred before and during
585 PCT-events. Median vertical trajectory paths during PRENUC and NUC times indicated air
586 coming from some 300 m above station level five days ago sinking to about one hundred
587 meters above station level during the last two days before arrival. The upper quartiles of the
588 PCT-height profiles point at strong subsidence before air mass arrival.

589 The right top panel in Fig. 5 maps average horizontal trajectory positions in 12 h steps in
590 months having at least ten PCT-events, i.e., May - September. Filled circles around the
591 trajectory positions comprise 95% of all events. The monthly average horizontal trajectory
592 direction during PCT-events mostly was from the northwest. In June and July the trajectories
593 reached farthest into the multiyear ice cover northeast of Greenland. Only during September
594 the back trajectories covered ice-free and marginal ice areas in the Fram Strait. We note that
595 the five-day back trajectories of PCT-events, (and of the other two approaches as well), stayed
596 within some 800 km of Mt. Zeppelin.

597

598

599 **3.2 The diameter growth (DGR) approach**

600

601 The DGR-approach to identify events of new particle formation builds on the classical
602 concept of particle growth through condensable vapors after an initial nucleation of sub-five
603 nanometer particles that cannot be observed with the available instrumentation, so called
604 “Banana-type” (Kulmala et al., 2004). The respective algorithm utilizes the parameter D50,
605 (see Table 1), and requires a growth of this diameter by at least a factor of 1.5 after the

606 nominal start of an event. With this threshold the algorithm searched through all 87646 hours
607 of the ten-year record and found 1199 DGR-events of new particle formation. After
608 eliminating cases of temporal overlap with the other two approaches 235 unique events of this
609 type remained, (see Table 2). Other or more DGR-events could have been found by
610 shortening the nominal nine NUC hours. For two reasons we refrained from discussing
611 shorter growth periods in the DGR-approach. Maintaining common-length NUC periods
612 facilitated the comparison of results of the three approaches. Furthermore, reducing the
613 growth period would also make PCT and DGR-events ever more similar.

614 Starting with an average value of $D_{50} \approx 16$ nm at the nominal start of DGR-events an
615 average growth rate of 1.8 nmh^{-1} is derived, which is in the range of $1 - 2 \text{ nmh}^{-1}$ derived by
616 Ström et al. (2009) for new particle formation in the lower boundary over Ny-Ålesund,
617 Spitsbergen but considerably lower than the maximum growth rate of 3.6 nmh^{-1} reported by
618 Asmi et al. (2016) for July at the Siberian station Tiksi at the coast of the Laptev Sea. [For](#)
619 [open ocean new particle formation events over the North Atlantic O'Dowd et al. \(2010\) report](#)
620 [a "typical growth rate" of \$0.8 \text{ nmh}^{-1}\$, whereas Ehn et al. \(2010\) give an average growth rate of](#)
621 [\$3 \text{ nmh}^{-1}\$. The average](#) length of DGR-events was 10 ± 1 h, (one standard deviation).

622 The average temporal development of the relative number size distribution during DGR-
623 events is presented in Fig. 4, (center). After a decrease of the sub-50 nm diameter median
624 from about 25 to 16 nm during the six hours before the nominal start of the events D_{50}
625 increases systematically during the following nine NUC hours with somewhat reduced growth
626 towards the end of the event.

627 During the PRENUC-periods particle number concentrations N_{300} , and the condensation
628 sink, (CS), decreased relative to the reference periods before and after the events.
629 Subsequently, during the NUC periods the strongest increases was found for N_{60} .
630 Environmental parameters around air mass arrival showed a strong lifting of cloud base,
631 (C25), and an extremely high increase in solar radiation, (by a factor of 11 during PRENUC

rev. 2017-2-18 10:48

Gelöscht: The

633 and by a factor of 60 during NUC periods). However, 12 h before air arrival precipitation had
634 been up by a factor of 2.5. Cloud fractions were down to about 70% of their reference values
635 24through 48 h before air arrival. Of the chemical aerosol parameters Na^+ and nssSO_4^{-2}
636 showed an increase of 2.6 and 2.3, respectively. OC12 and OC48 were slightly higher than
637 reference level before and during the events. Sea surface temperatures T24 were raised by
638 nearly one degree whereas earlier SST-values, (T36 – T5D), were up to one degree below
639 reference values.

640 Fig. 5, (left center panel), shows statistics of the vertical air movement before trajectory
641 arrival during DGR-events at Mt. Zeppelin covering a wide range of vertical movements
642 between 200 m and beyond 1500 m height. During the days when elevated DMSPt levels
643 were noted median trajectory heights were six to nine hundred meters. Median trajectories
644 during PRENUC times dipped down to the station level, (474 m a.s.l), about one day before
645 arrival, albeit lifted and subsided again shortly before arrival. Vertical trajectory pathways
646 will be discussed further in Section 4.2.

647 Monthly average trajectory positions and their variability in connection with DGR-events
648 are shown in Fig. 5, (center right panel). The months April through October had at least ten
649 DGR-events per month. As with PCT-events the general trajectory direction was from the
650 northwest, mostly staying for several days over the marginal ice zone between northeastern
651 Greenland and eastern Svalbard. During the earliest month of April with 14 DGR-events the
652 back trajectories reached farthest south into the ice-free parts of the Fram Strait.

653

654

655 **3.3 The Multiple-size approach (MEV)**

656

657 Leck and Bigg (2010) and Karl et al. (2013; 2012) discussed a type of new particle formation
658 that to date only has been reported from the summer Arctic. During these MEV-events high

659 ultrafine particle concentrations appear concurrently in a broad diameter range reaching from
660 under 10 to some 60 nm. We simulated this type in a search that required the concurrent
661 increase of NTO, N20, N40, and N60, (cf. Table 1), as averaged over the first three NUC
662 hours by a factor ≥ 1.6 over their respective averages during the six (PRENUC) hours. Over
663 the ten years of data 1191 such events of this type were identified, 266 of which remained
664 after removal of those overlapping with events of other approaches. During these unique
665 events the average concurrent concentration increase was 4.7 and the average length of the
666 events 12 ± 0.8 h.

667 The concurrent appearance of high concentrations at many particle sizes below 60 nm
668 resembles the nocturnal NPF-events analyzed by Suni et al. (2008) in the Australian
669 Eucalyptus forest and simulated in subsequent chamber experiments (Ristovski et al., 2010;
670 Junninen et al., 2008). We emphasize though that the condensing vapors in the Australian
671 NPF-events originating from terrestrial biogenic emission are quite different from the
672 polymer gels implicated in the Arctic MEV-events and originating from the surface
673 microlayer of the ocean.

674 The bottom part of Fig. 4 shows the average temporal development of relative number size
675 distributions before and during MEV-events. The development before the nominal start of
676 MEV-events is more complex than during the PRENUC-periods of the first two types of
677 events. Intermittently a mode around seven nanometers shows up that broadens and becomes
678 more prominent about two hours before the nominal start of events. The major PRENUC-
679 mode around 25 nm also broadens and becomes more prominent towards NUC. A weak
680 mode exists during PRENUC around 120 nm and hardly any particles beyond 400 nm. D50
681 sinks from 25 to about 20 nm and stays below 25 nm through the MEV-events even though
682 number concentrations increase during the first NUC-hours by more than a factor of five.

683 During NUC-periods all particle number concentrations increased, on average by a factor
684 of 1.6. Average solar radiation also increased by about 90% above reference level during

685 NUC-periods. Of the chemical parameters nssSO_4^{-2} showed an increase by a factor of three
686 during PRENUC and NUC-periods, and MSA a slight increase during PRENUC-periods. On
687 one hand, precipitation 12 h, and 36 to 48 h before trajectory arrival, (SP12, SP48), were
688 above reference levels for air arriving during PRENUC-periods. On the other hand, during
689 PRE, SP24, SP36, and SP5D indicated dry conditions during PRENUC and NUC-periods.
690 Only three to five days before air arrival slightly increased cloud fractions were noted. Sea
691 surface temperatures up to five days before trajectory arrival were on average about one
692 degree lower than their reference values. DMSpt parameters OC12 to OC36 were raised by
693 factors of 1.3 and 1.6 during PRENUC and NUC-periods, respectively.

694 Percentiles of vertical trajectory coordinates prior to and during MEV-events are displayed
695 in Fig. 5, (bottom left panel). During the events, and even stronger during the PRENUC
696 periods median trajectories had been below 500 m for more than four days. Furthermore, the
697 final air approach to Mt. Zeppelin mostly came from below the station level. Upper quartiles
698 of the vertical trajectory positions are substantially lower than with DGR-events. We note,
699 however, that a short excursion above station level occurred in the upper quartiles during the
700 last three hours before arrival.

701 The bottom right panel of Fig. 5 gives the monthly average trajectory positions and their
702 variability in connection with MEV-events. The months April through October had at least
703 ten MEV-events per month. As with the other approaches the general trajectory direction was
704 from the northwest, albeit with stronger swings towards the ice-free areas south of Svalbard
705 early and late in the season, (April, May, and September). Interestingly, the trajectories of the
706 11 MEV-events in October were directed nearly straight north from the North Pole.

707 Summarizing differences and commonalities among the results of the three approaches we
708 can state that the length of the events increases from four to ten and twelve, going from PCT
709 to MEV-events. PCT-events are characterized by lower-than-reference aerosol-chemical
710 parameters. Na^+ and nssSO_4^{-2} show strong increases in the other two types of events: Na^+ in

711 connection with DGR-events and nssSO_4^{-2} in connection with MEV-events. Both, PCT and
712 DGR-events exhibit strong increases in solar radiation. Precipitation before air arrival was
713 raised at varying times in connection with the three types of events. Cloudiness both
714 increased and decreased at varying times before air arrival with the three types of events.
715 Increased open water under the trajectories was strongest with DGR-events and least
716 important with MEV-events. Only in connection with PCT-events strongly raised sea surface
717 temperature were noted before trajectory arrival. DMSPt related ocean parameters were
718 raised to varying degrees and at varying times before all NPF-events, most strongly in
719 connection with PCT-events and least in connection with DGR-events.

720

721

722 4. Discussion

723

724 4.1. Environmental setting

725

726 The discussion of the results on new particle formation in the Svalbard region builds on the
727 variability of new particle formation and related environmental parameters on scales of
728 months, and days. Fig. 1 gives an overview over the geographic areas which were covered by
729 one, two, and five-day back trajectories to Mt. Zeppelin during the ten years of the present
730 study covering the months March through October. This figure illustrates that air arriving at
731 Mt. Zeppelin during the ten summers of the present study came from widely varying regions
732 from the central ice-covered Arctic via the northern seas and northernmost Scandinavia to
733 Greenland. One-day back trajectories cover a roundish area from the central east coast of
734 Greenland via northern Scandinavia to Franz-Josef-Land, North Pole and back to the north
735 coast of Greenland. Excluding inner Greenland this area is widened by roughly 500 km by 2-
736 day back trajectories and by at least another 500 km by 5-day back trajectories reaching over

rev. 2017-2-18 10:48

Gelöscht: bot

rev. 2017-2-18 10:48

Gelöscht:

739 most of Greenland and the adjacent seas west of Greenland. This is a much wider region
740 from which air may reach Mt. Zeppelin as compared to sites in the inner Arctic as illustrated
741 in Fig. 2 of Heintzenberg et al. (2015).

742 On the path of trajectories to Mt. Zeppelin quite different ice conditions were met (see,
743 Fig. 2). On average North Atlantic open waters reached around West Spitsbergen all the way
744 to Nordaustlandet. Drift ice was passed over by trajectories along the whole east coast of
745 Greenland. One-day trajectories passed over the marginal ice zone from the Fram Strait to
746 Franz-Josef Land but also over more contiguous ice close to the North Pole. At times, with
747 five-day back trajectories, even the marginal ice regions of Baffin Bay and Beaufort Sea were
748 reached.

749 The long-term geographical distribution of DMS_{Pt} in Fig. 3 reflects the water conditions
750 for phytoplankton biomass around Svalbard. Directly at the coasts of Greenland and Eurasia
751 increased nutrient availability in coastal and shelf waters (due to continental run-off and
752 enhanced hydrodynamics) cause localized areas of high DMS_{Pt} values. The low DMS_{Pt}
753 values further out along the coast of Greenland are due to sea ice reaching through the Fram
754 Strait far south, (see Fig. 2). A prominent feature in the regional DMS_{Pt} distribution is the
755 tongue of high DMS_{Pt}, (intense blue color), and thus high phytoplankton biomass east of this
756 area, reaching from Spitsbergen to roughly Jan Mayen that lies within one-day back
757 trajectories. Northward-flowing Atlantic waters, carried by the West Spitsbergen Current,
758 and southward-flowing fresh surface waters from melting ice, and recirculated Atlantic
759 waters, carried by the East Greenland Current (Rudels et al., 2005) are meeting. The layering
760 created by water masses of different density stabilizes the water column and traps
761 phytoplankton cells at well-lit depths. If sufficient nutrients are available, this can lead to the
762 development of large phytoplankton blooms, which can result in high concentrations of
763 DMS_{aq}, (see Fig. 2 in Leck and Persson, 1996a).

764 In the ten-year average cloud fractions systematic differences in cloudiness appear.
765 Depending on transport pathways as identified by the back trajectories, cloudiness varies on
766 the way to Spitsbergen. The ice-covered areas, (cf. Fig. 2), from the east coast of Greenland
767 to Franz-Josef-Land exhibit somewhat lower cloud fractions than the ice-free regions
768 southwest to east of Spitsbergen.

769

770

771 **4.2 Seasonal variability**

772

773 Seasonal changes are discussed in terms of monthly averages taken over the ten-year study
774 period. As expected in Earth's polar regions the seasonal variability of all environmental
775 parameters is very high as exemplified by the solar flux, (SFL), and the air temperature,
776 (TEM), at Mt. Zeppelin in Fig. 6. Due to the seasonal change in cloudiness, (cf. Fig. 7), the
777 seasonal distribution of SFL is not quite symmetrical about midsummer but is skewed slightly
778 towards the cloud minimum in spring. The air temperature, however, does not peak before
779 July and has a broad shoulder into fall and winter. The first, and partly absolute maxima, of
780 the seasonal distributions of NPF-events in Fig. 6 coincide with that of the SFL but then drop
781 of more slowly towards fall than solar radiation. In particular, MEV-events do so and even
782 have their main maximum in August. The occurrence of all NPF-events drops off sharply in
783 October. Whereas May as the first month with larger numbers of events is dominated by
784 PCT-events, followed by DGR and then MEV-events, the contributions of the three NPF-
785 types are reversed in the last month with high NPF-numbers, i.e., September.

786 Fig. 6 clearly shows that the formation of new particles in the Svalbard region is not
787 controlled by the late winter-to-early-spring phenomenon of Arctic haze peaking with highest
788 sulfate-concentrations in March, (cf. Fig. 3 in Heintzenberg, 1989, and Fig. 6), which has a
789 minimum in the total number of NPF-events. This minimum is in contrast with the maximum

790 in new particle formation rates found by Croft et al. (2016a) with their global aerosol model.
791 The high numbers of accumulation mode particles during the Arctic haze months in late
792 winter and spring yield the annual maximum in condensation sink, (CS in Fig. 6), which
793 could quench nucleation events and subsequent growth. Thus, even though photochemistry
794 may produce significant amounts of nucleating material, the freshly formed particles will not
795 grow to stable size before they are removed via either deposition or coagulation as discussed
796 by Tunved et al. (2013) and others. An alternative explanation of the late onset of NPF-
797 events in TNPF in spring lies in the marine biological processes not being activated nearby
798 during the Arctic haze period yet, (Heintzenberg and Leck, 1994).

799 Fig. 7 collects the seasonal variation of environmental parameters as averaged along the
800 back trajectories to Mt. Zeppelin. From their minimum in March-April open water conditions
801 improve until September, after which the pack ice extent under the trajectories rapidly
802 increases again. The widening open water areas are reflected in sea surface temperatures
803 under the trajectories that increase until September before they drop off strongly in October.
804 Consequently, because of its connection to marine biological activity DMSPt increases in the
805 euphotic zone from first photosynthetic light in May until it evens out around July and drops
806 off in October. Largest DMSPt values are reached in the vicinity of Svalbard, (cf. OC12 in
807 July and August in Fig. 7), i.e. considerably later than MSA. The ending of DMSPt-curves in
808 October is due to the lack of data not due to zero-DMSPt. Still, DMSPt concentrations are
809 expected to be low at this time of the year at temperate to polar latitudes due to low
810 phytoplankton biomass and low light exposure, (see Fig. 9 in Galí et al., 2015). In terms of
811 the MODIS-derived cloud fraction cloudiness increases rapidly from its minimum in April
812 and evens out on a plateau of 80 – 90% after July. The spring-minimum in cloudiness is
813 confirmed by the maximum in cloud base as indicated by C25 in Fig. 7. This seasonal
814 distribution of cloudiness does not correspond to the classical picture of near-surface
815 cloudiness that exhibits near cloud-free conditions in winter and mostly overcast with Arctic

rev. 2017-2-18 10:48

Gelöscht: (2013) and others.

817 stratus and fogs during the summer months (Warren and Hahn, 2002; Huschke, 1969). We
818 explain the difference by the specific atmospheric pathways covered by the back trajectories
819 of the present study (cf. Fig. 1). Trajectory-averaged precipitation parameters (SP12-5D in
820 Fig. 7) have minima in the period April – May, from which they increase towards their
821 maxima in fall and winter.

822 The chemical aerosol information derived from the analyses of filters samples has a
823 relatively low temporal resolution of at least one day combined with frequent gaps of several
824 days in between samples. Thus, it cannot directly be related to the time periods of NPF-
825 events. The seasonal distribution of chemical tracers, however, yields important information
826 about new particle formation. Taken over the whole year nssSO_4^{2-} in Fig. 6 is largely
827 anthropogenic, (Heintzenberg and Leck, 1994), and has its maximum during the peak of
828 Arctic haze in March and April and its minimum in August, which does not match any
829 seasonal distribution of NPF-events. We also plotted Na^+ in Fig. 6 as a tracer of the inorganic
830 marine aerosol components sea salt. Na^+ decreases from its winter maximum to its summer
831 minimum in June/July, again without similarity to the NPF-distributions. Instead, the
832 seasonal distribution of Na^+ rather closely follows that of the trajectory-derived wind speed
833 during the last hour before arrival, (not shown in the figure). Wind speed as driver for sea salt
834 production is a well established phenomenon (Blanchard and Woodcock, 1957). After a steep
835 rise in April MSA in Fig. 6 sharply peaks in May and then gradually drops off towards its
836 minimum in October, more gradually than reported for data taken from 1991 to 2004 by
837 Sharma et al. (2012) and earlier than reported by Heintzenberg and Leck (1994), both at the
838 same station. Our seasonal distribution of MSA most closely resembles that of SFL, in Fig. 6,
839 albeit with its peak in May a month earlier than SFL and more strongly skewed towards
840 spring. According to Leck and Persson (1996b) on average the concentrations of the marine
841 biogenic sulfur components, (DMS and MSA), fell with a decline rate of about 30% per week

842 approaching zero values in September explained by reduced ppp (Leck and Persson, (1996a),
843 (consistent with Becagli et al., 2016).

844 As MSA is the only measured aerosol component with exclusively marine biogenic
845 sources, we illustrate its seasonal distribution in greater detail in Fig. 8. In this figure MSA-
846 concentrations measured on Mt. Zeppelin have been extrapolated along 5-day back
847 trajectories, forming monthly average monthly maps of potential MSA-sources during the
848 biologically most active months of March through October.

849 Fig. 8 yields several pieces of information that are relevant to the issue of new particle
850 formation. Early in spring the biological aerosol sources are limited to the North Atlantic and
851 Norwegian Sea. In April the tongue of newly opened waters between Novaya Zemlya and
852 Franz-Josef-Land seemingly is beginning to become biologically active. In May this area
853 widens towards the Barents Sea while the North Atlantic also becomes more active, reaching
854 the Fram Strait. In August two wide potential source regions cover the region from Northern
855 Greenland to the northern end of Scandinavia and the region Barents to Kara Sea. In
856 September even the pack ice north of Svalbard becomes biologically active, (Leck and
857 Persson, 1996a), and shows potential MSA sources, in particular, north of the northern coast
858 of Greenland. Finally, the very weak potential MSA sources in October appear to be situated
859 mainly over the Kara Sea and over the North Atlantic.

860 How do these seasonal distributions compare to those of the NPF-events identified by the
861 three search-approaches defined in Section 3? To address this question we constrained the
862 average seasonal distribution of environmental parameters to those hours that had been
863 identified by the NPF-events of the three approaches. However, none of the individual
864 seasonal distributions of constrained environmental parameters follows closely any of the
865 NPF-events. In particular, the main MSA peak remains in May, thus one month earlier than
866 any peak of the NPF-occurrences. To elucidate further potential differences in the three types
867 of NPF-events we return to the discussion of vertical pathways of related back trajectories,

rev. 2017-2-18 10:48

Gelöscht: items

869 (see Fig. 5). In this figure all three types of NPF-events exhibit a wide range of vertical
870 trajectory paths. As we expect the regional sources of primary particles and particle
871 precursors to be at or near the surface we segregated the NPF-events into subpopulations with
872 back trajectories that remained a given time below 500 m, (roughly station level). In Fig. 9
873 we collected the results concerning the 93 NPF-events that occurred with trajectories under
874 the 500 m limit, i.e., roughly 12% of all events. The top panel shows that the related
875 trajectories not only stayed below 500 m through most of the last five days before arrival but
876 close to the surface until they started rising to the station level about 24 h before arrival. The
877 peak of the sum of event occurrences now coincided with the main MSA peak in May, (see
878 center panel in Fig. 9). For DGR-events the May-maximum was particularly strong whereas
879 the PCT-predominantly occurred in May and June and MEV-events remained clustered
880 around the later part of summer, possibly coupled to SST and DMSPt.

881 A number of environmental parameters indicated substantial deviations from their
882 respective reference values during the months with most frequent occurrence of this sub-
883 population of NPF-events. Strongest deviations were noted for precipitation that was elevated
884 above reference levels two to five days before trajectory arrival, most prominently for DGR-
885 events in May, (by a factor of six 36 h before trajectory arrival). Strong positive deviations in
886 aerosol-chemical parameters only occurred with Na⁺ in PCT and MEV-events, indicating
887 relatively high wind speeds near sea surface in the related air masses. MSA was elevated up
888 to 50% above reference levels only during MEV-events. Elevated levels of DMSPt were
889 noted with all three types of NPF-formation, most prominently for DGR-events 12 to 36
890 hours before which DMSPt was increased by a factor up to 1.7 relative to reference levels.

891 The bottom panel of Fig. 9 gives average trajectory positions in 12 h steps for the months
892 May through September. The circles around the steps comprise 95% of all trajectories.
893 During all months the trajectories stayed in the ice-free and marginal ice zone between Fram
894 Strait and Eastern Svalbard as illustrated by average July ice cover for the ten study years,

rev. 2017-2-18 10:48

Gelöscht:

rev. 2017-2-18 10:48

Gelöscht: raised

rev. 2017-2-18 10:48

Gelöscht: factors

898 (for average monthly ice covers cf. Fig. 8). In particular during the earliest and latest months
899 of May and September the trajectories swing farthest south over the open water south of
900 Svalbard. We note that the complementary sub-population of results with trajectories
901 remaining above station level did not yield results that differed strongly from those for the
902 whole population of back trajectories.

903 As a last step in the discussion of seasonal variations in new particle formation a model is
904 formulated that describes the average sum of NPF-events, (TNPF), as a function of three
905 parameters, two of which are directly measurable at the site. With the linear combination of
906 the solar flux, (SFL, Wm^{-2}), average sea surface temperature under back trajectories 36 to 48
907 hours before their arrival at the site, (T48, $^{\circ}\text{C}$), and condensation sink, (CS, 10^5 s^{-1}):

908

$$909 \quad TNPF = 0.57 \cdot SFL + 15.4 \cdot T48 - 0.69 \cdot CS$$

910

911 TNPF as shown in Fig. 10, can be described within an average deviation of 5% taken over the
912 major months with new particle formation, April - October. Any other of the sea surface
913 parameters describes TNPF less satisfactorily,

914

915

916

917

918 **4.3 Diurnal variability**

919

920 Average hourly occurrence of the three types of NPF-events is plotted in Fig. 11, (top). The
921 three approaches yield rather similar diel variations. From their minimum during the night
922 and early morning hours they reach their maximum occurrence between 12 and 16 h UTC in
923 the afternoon. One might expect the differences between the NPF-types to be due to the

rev. 2017-2-18 10:48

Gelöscht: well

925 requirement of the three types of NPF formation being mutually exclusive. However, this
926 constraint does not exclude that they occur at the same time of day, only that they occur at the
927 same time on the same day.

928 Over the continents new particle formation and growth events of the classical “Banana-
929 type” usually exhibit an increase in measurable precursors such as sulfuric acid shortly after
930 sunrise followed by the detection of increased numbers of nanometer-sized particles between
931 one and two hours later (Kulmala et al., 2004), who deduce a connection to photochemically
932 produced condensable vapors from this daily pattern. In the Svalbard region the sun is up all
933 day between mid-April and the end of August. Consequently we would expect the
934 photochemical production of condensable vapors to have a smaller diurnal amplitude than at
935 lower latitudes, which in turn should even out the diurnal pattern of NPF-events to some
936 degree. Despite the relatively small daily variations in solar elevations the solar flux on Mt.
937 Zeppelin varied on average by more than a factor of five during the sunlit days (see curve
938 SFL in Fig. 11, bottom). The daily maximum of SFL between 12 and 15 UTC coincides well
939 with the average diel change in N25 and NPF-occurrence. As expected in particle growth due
940 to condensable vapors after initial nucleation the daily maximum in N10 precedes that of N25
941 by a few hours.

942 The other process controlling the development of newly formed small particles is the
943 diurnal development of the planetary boundary layer, (Kulmala et al., 2004). We have no
944 data on the daily variation in boundary layer structure over or near the measurement site. The
945 ceilometer data yield the only high-resolution information with some connection to the
946 structure of the planetary boundary layer. During the summer months these data show a
947 consistent daily variation with a jump in most frequent hourly cloud base by about 100 m
948 from about 1570 m after 09 UTC with rather stable values following until 16 UTC, after
949 which cloud base decreases again to values comparable to the early morning hours. The
950 hourly medians of the vertical displacement parameter DZ, (see Fig. 11, bottom), provide a

951 clearer diurnal variation. While being negative throughout the day, i.e. indicating subsiding
952 air during the last hour before arrival at Mt. Zeppelin, DZ indicates the weakest subsidence in
953 early afternoon. We interpret diurnal variation in cloud base and DZ as indicative of local
954 clearing and convection during the day that may be conducive to photochemical processes
955 and mixing in the boundary layer, both of which would be enhancing new particle formation.

956

957

958 | 5. Summary and conclusions

959

960 Three different types of events of new particle formation, (NPF), were identified through
961 objective search algorithms formulated for the present study. The first and simplest algorithm
962 utilizes short-term increases in particle concentrations below 25 nm, (PCT-events). The
963 second one builds on the growth of the sub-50 nm diameter-median, (DGR-events), and is
964 most closely related to the classical “banana-type” of events, (Kulmala et al., 2004) involving
965 the presence of photochemically generated DMS oxidation precursors. The third and most
966 complex, so-called multiple-size approach to identifying NPF-events builds on the hypothesis
967 of Leck and Bigg (2010), suggesting the concurrent production of polymer gel particles at
968 several sizes below about 60 nm, (MEV-events).

969 With these algorithms NPF-events were identified in a ten-year record of hourly number-
970 size distributions taken at the research station on Mt. Zeppelin, Spitsbergen. As a first and
971 general conclusion we can state that NPF-events are a summer phenomenon and not related to
972 Arctic haze, which is a late winter-to-early spring event. The seasonal distribution of the
973 available information on cloudiness does not suggest any direct connection with NPF-
974 formation. The MODIS derived cloud fraction generally is very high (70 – 90%) and rather
975 evenly distributed over the Svalbard region during the months with high frequencies of NPF-
976 events. As already reported in Tunved et al. (2013), NPF-events appear to be somewhat

rev. 2017-2-18 10:48

Gelöscht: Conclusions

rev. 2017-2-18 10:48

Gelöscht: (2013)

979 sensitive to the available data on precipitation derived from the trajectory model, in particular
980 when constrained to cases with back trajectories staying below 500 m. In this subpopulation
981 of NPF-events DGR-events show the strongest change in precipitation parameters in
982 connection with new particle formation.

983 The seasonal distribution of solar flux suggests some photochemical control that may
984 affect marine biological processes generating particle precursors and/or atmospheric
985 photochemical processes that generate condensable vapors from precursor gases. Whereas
986 the seasonal distribution of the biogenic MSA follows that of the solar flux it peaks before the
987 maxima in NPF-occurrence. For PCT-events, and more distinctly so for DGR-events, this
988 one-month delay disappears in the subpopulation with back trajectories staying below 500 m.
989 MEV-events, however, maintain their peak occurrence later in summer and early fall.

990 With the limited information on particle size, composition, particle precursors, and
991 environmental conditions no definitive statements can be made about the processes leading to
992 the formation of new particles in the Svalbard region. A host of findings, however, point to
993 varying and rather complex marine biological source processes. The potential source regions
994 for all types of new particle formation appear to be restricted to the marginal ice and open
995 water areas between Northeastern Greenland and Eastern Svalbard. During earliest and latest
996 months with high numbers of NPF-events the back trajectories reach farther south into the
997 open waters of the North Atlantic. Depending on conditions yet to be clarified new particle
998 formation may become visible as short bursts of particles around 20 nm, (PCT-events), longer
999 events involving condensation growth, (DGR-events), or extended events with elevated
1000 concentrations of particles at several sizes below 100 nm, (MEV-events). The seasonal
1001 distribution of NPF-events peaks later than that of MSA and, DGR and in particular of MEV-
1002 events reach into late summer and early fall with much open, warm, and DMSPt-rich waters
1003 around Svalbard, promoting the production of *Phaeocystis pouchetii* together with polymer
1004 gels. Consequently, a simple model to describe the seasonal distribution of the total number

1005 of NPF-events can be based on solar flux, and sea surface temperature, representing
1006 environmental conditions for marine biological activity, and condensation sink, controlling
1007 the balance between new particle nucleation and their condensational growth. Based on the
1008 sparse knowledge about the seasonal cycle of gel-forming marine microorganisms and their
1009 controlling factors we hypothesize that the seasonal distribution of DGR and more so MEV-
1010 events reflect the seasonal cycle of the gel-forming phytoplankton.

1011 Despite the rather small diel changes expected during the summer Arctic there is a
1012 significant diurnal variation in aerosol and environmental parameters. Diurnal distributions
1013 of particle numbers below ten, (N10), and below 25 nm, (N25) follow that of the solar flux
1014 rather closely with a maximum between 14 and 16 UTC with the maximum of N10 occurring
1015 a few hours before that of N25. This delay in maxima may be caused by a slow particle
1016 growth due to photochemically produced condensable vapors. With a peak around noon
1017 MEV-events show the earliest daily peak occurrence with PCT and DGR-events peaking
1018 between 15 and 17 h, more closely to the maximum solar flux. Considering the diurnal
1019 variation in vertical trajectory displacement, (DZ), the early daily maximum in MEV-
1020 occurrence may be simply controlled by boundary layer dynamics.

1021 With the large database of ten years of aerosol data on Mt. Zeppelin enriched by
1022 environmental atmospheric and marine data occurrences, pathways and potential source areas
1023 of different types of new particle formation in the Svalbard region were elucidated by the
1024 present study. More process related information about new particle formation would require
1025 dedicated mechanistic experiments with more detailed information on particle precursors,
1026 ultrafine particles, and boundary layer mixing processes. DGR and MEV-types of new
1027 particle formation seem to be more closely related to near-surface processes. Thus, a low-
1028 level site such as the reopened Station Nord, (Nguyen et al., 2016), would be more suitable
1029 for related mechanistic experiments. Station Nord has the additional advantage of being close
1030 to the potential source regions of DGR and MEV-events identified by the present study.

1031 Acknowledgements

1032

1033 The back trajectories created through the local use of the [HYSPLIT4](#) model developed,
1034 maintained and generously distributed by the Air Resources Laboratory of NOAA were a

1035 backbone of the present study. We are very grateful for the ceilometer data provided by the
1036 Alfred-Wegener- Institute in Bremerhaven/Potsdam and to NSIDC for their providing daily

1037 Arctic sea ice data. Complementing our own chemical analyses of Mt. Zeppelin filter data,
1038 sodium and sulfate results were taken from the EBAS database at the Norwegian Institute for

1039 Air Research (<http://ebas.nilu.no>), for which we are indebted to Anne-Gunn Hjellbrekke and
1040 Wenche Aas. We thank the NASA Ocean Biology Distributed Active Archive Center

1041 (OB.DAAC) for access to MODIS datasets. We are indebted to Yafang Cheng and Zhibin
1042 Wang for providing the algorithm for calculating the condensation sink. MG acknowledges

1043 the receipt of a Beatriu de Pinós post-doctoral fellowship funded by the Generalitat de
1044 Catalunya. Long-term funding of the DMPS measurements was provided by the Swedish

1045 Environmental Protection Agency (Naturvårdsverket). We also thank Norwegian Polar
1046 Institute for substantial support of the field operation on Mt. Zeppelin.

1047

1048

rev. 2017-2-18 10:48
Gelöscht: ... [2]

rev. 2017-2-18 10:48
Gelöscht: HYSPLIT

rev. 2017-2-18 10:48
Gelöscht: most

Literature

- 1053
 1054
 1055 Agarwal, J. K., and Sem, G. J.: Continuous flow, single-particle-counting condensation
 1056 nucleus counter, *J. Aerosol Sci.*, 11, 343-357, 1980.
- 1057 An, N., and Wang, K.: A Comparison of MODIS-Derived Cloud Fraction with Surface
 1058 Observations at Five SURFRAD Sites, *J. Appl. Meteor. Clim.*, 54, 1009-1020, 2015.
- 1059 Asmi, E., Kondratyev, V., Brus, D., Laurila, T., Lihavainen, H., Backman, J., Vakkari, V.,
 1060 Aurela, M., Hatakka, J., Viisanen, Y., Uttal, T., Ivakhov, V., and Makshatas, A.:
 1061 Aerosol size distribution seasonal characteristics measured in Tiksi, Russian Arctic,
 1062 *Atmos. Chem. Phys.*, 16, 1271-1287, 10.5194/acp-16-1271-2016, 2016.
- 1063 Ayers, G. P., Cainey, J. M., Granek, H., and Leck, C.: Dimethylsulfide oxidation and the ratio
 1064 of methansulfonate to non sea-salt sulfate in the marine aerosol, *J. Atmos. Chem.*, 25,
 1065 307-325, 1996.
- 1066 [Bates, T. S., Johnson, J. E., Quinn, P. K., Goldan, P. D., Kuster, W. C., Covert, D. C., and](#)
 1067 [Hahn, C. J.: The biogeochemical sulfur cycle in the marine boundary layer over the](#)
 1068 [Northeast Pacific Ocean, *J. Atmos. Chem.*, 10, 59-81, 1990.](#)
- 1069 Becagli, S., Lazzara, L., Marchese, C., Dayan, U., Ascanius, S. E., Cacciani, M., Caiazzo, L.,
 1070 Di Biagio, C., Di Iorio, T., di Sarra, A., Eriksen, P., Fani, F., Giardi, F., Meloni, D.,
 1071 Muscari, G., Pace, G., Severi, M., Traversi, R., and Udisti, R.: Relationships linking
 1072 primary production, sea ice melting, and biogenic aerosol in the Arctic, *Atmos.*
 1073 *Environ.*, 136, 1-15, <http://dx.doi.org/10.1016/j.atmosenv.2016.04.002>, 2016.
- 1074 Beine, H. J., Argentini, S., Maurizi, A., Mastrantonio, G., and Viola, A.: The local wind field
 1075 at Ny-Ålesund and the Zeppelin mountain at Svalbard, *Meteorol. Atmos. Phys.*, 78,
 1076 107-113, 2001.
- 1077 Bélanger, S., Babin, M., and Tremblay, J.-É.: Increasing cloudiness in Arctic damps the
 1078 increase in phytoplankton primary production due to sea ice receding, *Biogeosciences*,
 1079 doi:10.5194/bg-5110-4087-2013, 2013.
- 1080 Blanchard, D. C., and Woodcock, A. H.: Bubble formation and modification in the sea and its
 1081 meteorological significance, *Tellus*, 9, 145-158, 1957.
- 1082 Browse, J., Carslaw, K. S., Mann, G. W., Birch, C. E., Arnold, S. R., and Leck, C.: The
 1083 complex response of Arctic aerosol to sea-ice retreat, *Atmos. Chem. Phys.*, 14, 7543-
 1084 7557, 10.5194/acp-14-7543-2014, 2014.
- 1085 Charlson, R. J., Lovelock, J. E., Andreae, M. O., and Warren, S. G.: Oceanic phytoplankton,
 1086 atmospheric sulphur, cloud albedo and climate, *Nature*, 326, 655-661, 1987.

1087 Croft, B., Martin, R. V., Leaitch, W. R., Tunved, P., Breider, T. J., D'Andrea, S. D., and
1088 Pierce, J. R.: Processes controlling the annual cycle of Arctic aerosol number and size
1089 distributions, *Atmos. Chem. Phys.*, 16, 3665-3682, 10.5194/acp-16-3665-2016, 2016a.

1090 Croft, B., Wentworth, G. R., Martin, R. V., Leaitch, W. R., Murphy, J. G., Murphy, B. N.,
1091 Kodros, J. K., Abbatt, J. P. D., and Pierce, J. R.: Contribution of Arctic seabird-colony
1092 ammonia to atmospheric particles and cloud-albedo radiative effect, *Nature*
1093 *Communications*, 7, 13444, 10.1038/ncomms13444
1094 <http://www.nature.com/articles/ncomms13444-supplementary-information>, 2016b.

1095 Dal Maso, M., Kulmala, M., Riipinen, I., Wagner, R., Hussein, T., Aalto, P. P., and Lehtinen,
1096 K. E. J.: Formation and growth of fresh atmospheric aerosols: eight years of aerosol
1097 size distribution data from SMEAR II, Hyytiälä, Finland, *Bor. Env. Res.*, 10, 323-336,
1098 2005.

1099 Das, R., Granat, L., Leck, C., Praveen, P. S., and Rodhe, H.: Chemical composition of
1100 rainwater at Maldives Climate Observatory at Hanimaadhoo (MCOH), *Atmos. Chem.*
1101 *Phys.*, 11, 3743-3755, 10.5194/acp-11-3743-2011, 2011.

1102 Dee, D. P., Uppala, S. M., Simmons, A. J., Berrisford, P., Poli, P., Kobayashi, S., and
1103 Bechtold, P.: The ERA - Interim reanalysis: Configuration and performance of the
1104 data assimilation system, *Q. J. Roy. Meteorol. Soc.*, 137, 553-597, 2011.

1105 Draxler, R., and Rolph, G.: HYSPLIT (HYbrid Single-Particle Lagrangian Integrated
1106 Trajectory) Model access via NOAA ARL READY, NOAA Air Resources
1107 Laboratory, Silver Spring, MD, 2003.

1108 [Ehn, M., Vuollekoski, H., Petäjä, T., Kerminen, V.-M., Vana, M., Aalto, P., de Leeuw, G.,](#)
1109 [Ceburnis, D., Dupuy, R., O'Dowd, C. D., and Kulmala, M.: Growth rates during](#)
1110 [coastal and marine new particle formation in western Ireland, *J. Geophys. Res.*, 115,](#)
1111 [n/a-n/a, 10.1029/2010JD014292, 2010.](#)

1112 Flyger, H., and Heidam, N. Z.: Ground level measurements of the summer tropospheric
1113 aerosol in Northern Greenland, *J. Aerosol Sci.*, 9, 157-168, 1978.

1114 Galí, M., Devred, E., Levasseur, M., Royer, S.-J., and Babin, M.: A remote sensing algorithm
1115 for planktonic dimethylsulfoniopropionate (DMSP) and an analysis of global patterns,
1116 *Remote Sens. Environ.*, 171, 171-184, <http://dx.doi.org/10.1016/j.rse.2015.10.012>,
1117 2015.

1118 Galí, M., and Simó, R.: A meta - analysis of oceanic DMS and DMSP cycling processes:
1119 Disentangling the summer paradox, *Global Biochem. Cycles*, 29, 496-515, 2015.

1120 Gao, Q., Leck, C., Rauschenberg, C., and Matrai, P. A.: On the chemical dynamics of
1121 extracellular polysaccharides in the high Arctic surface microlayer, *Ocean Sci.*
1122 *Discuss.*, 9, 215–259, 2012.

1123 Heintzenberg, J., Bischof, W., Odh, S.-Å., and Moberg, B.: An investigation of possible sites
1124 for a background monitoring station in the European Arctic., *International*
1125 *Meteorological Institute in Stockholm, Department of Meteorology, Stockholm*
1126 *University, Stockholm, Report Nr. AP-22, 74 pp, 1983.*

1127 Heintzenberg, J., and Larssen, S.: SO₂ and SO₄ in the Arctic: Interpretation of observations at
1128 three Norwegian Arctic-subArctic stations, *Tellus*, 35B, 255-265, 1983.

1129 Heintzenberg, J.: Arctic haze: air pollution in polar regions, *AMBIO*, 18, 50-55, 1989.

1130 Heintzenberg, J., and Leck, C.: Seasonal variation of the atmospheric aerosol near the top of
1131 the marine boundary layer over Spitsbergen related to the Arctic sulphur cycle, *Tellus*,
1132 46B, 52-67, 1994.

1133 Heintzenberg, J., Leck, C., Birmili, W., Wehner, B., Tjernström, M., and Wiedensohler, A.:
1134 Aerosol number-size distributions during clear and fog periods in the summer high
1135 Arctic: 1991, 1996, and 2001, *Tellus*, 58B, 41-50, 2006.

1136 Heintzenberg, J., Wehner, B., and Birmili, W.: "How to find bananas in the atmospheric
1137 aerosol" New approach for analyzing atmospheric nucleation and growth events,
1138 *Tellus B*, 59, 273-282, 2007.

1139 Heintzenberg, J.: The aerosol-cloud-climate conundrum, *IJGW*, 4, 219-241, 2012.

1140 Heintzenberg, J., Leck, C., and Tunved, P.: Potential source regions and processes of aerosol
1141 in the summer Arctic, *Atmos. Chem. Phys.*, 15, 6487-6502, [10.5194/acp-15-6487-](https://doi.org/10.5194/acp-15-6487-2015)
1142 [2015](https://doi.org/10.5194/acp-15-6487-2015), 2015.

1143 Held, A., Brooks, I. M., Leck, C., and Tjernström, M.: On the potential contribution of open
1144 lead particle emissions to the central Arctic aerosol concentration, *Atmos. Chem.*
1145 *Phys.*, 11, 3093-3105, [10.5194/acp-11-3093-2011](https://doi.org/10.5194/acp-11-3093-2011), 2011a.

1146 Held, A., Orsini, D. A., Vaattovaara, P., Tjernström, M., and Leck, C.: Near-surface profiles
1147 of aerosol number concentration and temperature over the Arctic Ocean, *Atmos.*
1148 *Meas. Tech.*, 4, 1603–1616, 2011b.

1149 Hubanks, P., Platnick, S., King, M., and Ridgway, B.: MODIS Atmosphere L3 Gridded
1150 Product Algorithm Theoretical Basis, Document (ATBD) and Users Guide, 2015.

1151 Huschke, R. E.: Arctic cloud statistics from "air calibrated" surface weather observations,
1152 *Rand Corporation Memo. RM 6173-PR, 79 pp, 1969.*

- 1153 IOCCG: Ocean Colour Remote Sensing in Polar Seas, Report 16, Eds. Babin, M., Arrigo, K.,
1154 Bélanger, S. and Forget, M.-H., 129 pp, 2015.
- 1155 Jaenicke, R., and Schütz, L.: Arctic aerosols in surface air, *Idöjaras*, 86, 235-241, 1982.
- 1156 Junge, C. E.: Air chemistry and Radioactivity, Academic Press, New York and London, 382
1157 pp., 1963.
- 1158 [Junninen, H., Hulkkonen, M., Riipinen, I., Nieminen, T., Hirsikko, A., Suni, T., Boy, M., Lee,](#)
1159 [S.-H., Vana, M., Tammet, H., Kerminen, V.-M., and Kulmala, M.: Observations on](#)
1160 [nocturnal growth of atmospheric clusters, *Tellus B*, 60, 365-371, 2008.](#)
- 1161 [Karl, M., Gross, A., Leck, C., and Pirjola, L.: Intercomparison of dimethylsulfide oxidation](#)
1162 [mechanisms for the marine boundary layer: Gaseous and particulate sulfur](#)
1163 [constituents, *J. Geophys. Res.*, 112, D15304, 10.1029/2006JD007914, 2007.](#)
- 1164 Karl, M., Leck, C., Gross, A., and Pirjola, L.: A Study of New Particle Formation in the
1165 Marine Boundary Layer Over the Central Arctic Ocean using a Flexible
1166 Multicomponent Aerosol Dynamic Model, *Tellus*, 64B,
1167 doi:<http://dx.doi.org/10.3402/tellusb.v3464i3400.17158>, 2012.
- 1168 Karl, M., Leck, C., Coz, E., and Heintzenberg, J.: Marine nanogels as a source of atmospheric
1169 nanoparticles in the high Arctic, *Geophys. Res. Lett.*, 40, 3738–3743, DOI:
1170 10.1002/grl.50661, 2013.
- 1171 Keene, W. C., Pszenny, A. A. P., Galloway, J. N., and Hawley, M. E.: Sea-salt corrections
1172 and interpretation of constituent ratios in marine precipitation, *J. Geophys. Res.*, 91,
1173 6647-6658, 1986.
- 1174 Keller, M. D., Bellows, W. K., and Guillard, R. R. L.: A survey of dimethylsulfide production
1175 in 12 classes of marine phytoplankton, in: Biogenic sulfur in the environment, edited
1176 by: E.S. Saltzman, and Cooper, W. J., American Chemical Society, Washington, D,
1177 167–182, 1989.
- 1178 King, M. D., Platnick, S., Menzel, W. P., Ackerman, S. A., and Hubanks, P. A.: Spatial and
1179 temporal distribution of clouds observed by MODIS onboard the Terra and Aqua
1180 satellites, *IEEE Trans. Geosci. Remote Sens.*, 51, 3826–3852, 2013.
- 1181 Knutson, E. O., and Whitby, K. [T.: Accurate Measurement of Aerosol Electrical Mobility](#)
1182 [Moments, *J. Aerosol Sci.*, 6, 453-460, 1975a.](#)
- 1183 [Knutson, E. O., and Whitby, K. T.:](#) Aerosol classification by electric mobility: apparatus,
1184 theory, and applications, *J. Aerosol Sci.*, 6, 443-451, [1975b](#),

rev. 2017-2-18 10:48

[1] verschoben (Einfügung)

rev. 2017-2-18 10:48

Gelöscht: 1975a

1186 | Kulmala, M., Dal Maso, M., Mäkelä, J. M., Pirjola, L., Väkevä, M., Aalto, P. P.,
1187 | Miikkulainen, P., Hämeri, K., and O'Dowd, C. D.: On the formation, growth and
1188 | composition of nucleation mode particles, *Tellus*, 53B, 479-490, 2001.
1189 | Kulmala, M., Vehkamäkia, H., Petäjä, T., Dal Maso, M., Lauri, A., Kerminen, V.-M., Birmili,
1190 | W., and McMurry, P. H.: Formation and growth rates of ultrafine atmospheric
1191 | particles: a review of observations, *J. Aerosol Sci.*, 35, 143-176, 2004.
1192 | Lana, A., Simó, R., Vallina, S. M., and Dachs, J.: Re-examination of global emerging patterns
1193 | of ocean DMS concentration, *Biogeochem.*, 110, 173-182, 2012.
1194 | Lannefors, H., Heintzenberg, J., and Hansson, H.-C.: A comprehensive study of physical and
1195 | chemical parameters of the Arctic summer aerosol; results from the Swedish
1196 | expedition Ymer-80, *Tellus*, 35B, 40-54, 1983.
1197 | Leck, C., and Persson, C.: The central Arctic Ocean as a source of dimethyl sulfide: Seasonal
1198 | variability in relation to biological activity, *Tellus*, 48B, 156-177, 1996a.
1199 | Leck, C., and Persson, C.: Seasonal and short-term variability in dimethyl sulfide, sulfur
1200 | dioxide and biogenic sulfur and sea salt aerosol particles in the arctic marine boundary
1201 | layer, during summer and autumn, *Tellus*, 48B, 272-299, 1996b.
1202 | Leck, C., and Bigg, E. K.: Aerosol production over remote marine areas - A new route,
1203 | *Geophys. Res. Lett.*, 23, 3577-3581, 1999.
1204 | Leck, C., and Bigg, E. K.: New particle formation of marine biological origin, *Aerosol Sci.*
1205 | *Technol.*, 44, 570-577, 2010.
1206 | Leck, C., Gao, Q., Mashayekhy Rad, F., and Nilsson, U.: Size-resolved atmospheric
1207 | particulate polysaccharides in the high summer Arctic, *Atmos. Chem. Phys.*, 13,
1208 | 12573-12588, 10.5194/acp-13-12573-2013, 2013.
1209 | Lindsay, R., Wensnahan, M., Schweiger, A., and Zhang, J.: Evaluation of seven different
1210 | atmospheric reanalysis products in the Arctic, *J. Clim.*, 27, 2588-2606, 2014.
1211 | Liss, P. S., and Merlivat, L.: Air-sea gas exchange rates: Introduction and synthesis, in: *The*
1212 | *Role of Air-Sea Exchange in Geochemical Cycling*, edited by: Buat-Menard, P.,
1213 | Reidel, Norwell, MS, 113-127, 1986.
1214 | Maritorena, S., Siegel, D. A., and Peterson, A. R.: Optimization of a semianalytical ocean
1215 | color model for global-scale applications, *Appl. Opt.*, 41.15, 2705-2714, 2002.
1216 | Matrai, P. A., and Vernet, M.: Dynamics of the vernal bloom in the marginal ice zone of the
1217 | Barents Sea: Dimethyl sulfide and dimethylsulfoniopropionate budgets, *Journal of*
1218 | *Geophysical Research: Oceans*, 102, 22965-22979, 10.1029/96JC03870, 1997.

rev. 2017-2-18 10:48

Gelöscht: Knutson, E. O., and Whitby, K.

rev. 2017-2-18 10:48

[1] nach oben verschoben: T.:
Accurate Measurement of Aerosol Electrical
Mobility Moments, *J. Aerosol Sci.*, 6, 453-
460,

rev. 2017-2-18 10:48

Gelöscht: 1975b. -

1225 Nguyen, Q. T., Glasius, M., Sørensen, L. L., Jensen, B., Skov, H., Birmili, W., Wiedensohler,
1226 A., Kristensson, A., Nøjgaard, J. K., and Massling, A.: Seasonal variation of
1227 atmospheric particle number concentrations, new particle formation and atmospheric
1228 oxidation capacity at the high Arctic site Villum Research Station, Station Nord,
1229 Atmos. Chem. Phys., 16, 11319–11336, 10.5194/acp-2016-205, 2016.

1230 Norman, A. L., Barrie, L. A., Toom-Sauntry, D., Sirois, A., Krouse, H. R., Li, S. M., and
1231 Sharma, S.: Sources of aerosol sulphate at Alert: Apportionment using stable isotopes,
1232 J. Geophys. Res., 104, 11619-11631, 1999.

1233 [O'Dowd, C., Monahan, C., and Dall'Osto, M.: On the occurrence of open ocean particle](#)
1234 [production and growth events, Geophys. Res. Lett., 37, L19805,](#)
1235 [doi:19810.11029/12010GL044679, 2010.](#)

1236 Orellana, M. V., Matrai, P. A., Janer, M., and Rauschenberg, C. D.:
1237 Dimethylsulfoniopropionate storage in *Phaecystis* (Prymnesiophyceae) secretory
1238 vesicles J. Phycol., 47, 112-117, 10.1111/j.1529-8817.2010.00936.x, 2011a.

1239 Orellana, M. V., Matrai, P. A., Leck, C., Rauschenberg, C. D., Lee, A. M., and Coz, E.:
1240 Marine microgels as a source of cloud condensation nuclei in the high Arctic, PNAS,
1241 108, 13612–13617, 2011b.

1242 Pirjola, L., Kulmala, M., Wilck, M., Bischoff, A., Stratmann, F., and Otto, E.: Formation of
1243 sulphuric acid aerosols and cloud condensation nuclei: An expression for significant
1244 nucleation and model comparison, J. Aerosol Sci., 30, 1079-1094, 1999.

1245 Polissar, A. V., Hopke, P. K., Paatero, P., Kaufman, Y. J., Hall, D. K., Bodhaine, B. A.,
1246 Dutton, E. G., and Harris, J. M.: The aerosol at Barrow, Alaska: long-term trends and
1247 source locations, Atmos. Environ., 33, 2441-2458, 1999.

1248 Rahn, K. A., and Shaw, G. E.: Particulate air pollution in the Arctic: Large-scale occurrence
1249 and meteorological controls, in: Atmospheric Aerosols and Nuclei, edited by: Roddy,
1250 F., and O'Connor, T. C., Dept. of Physics, University College, Galway, Ireland 21-27
1251 Sept., 223-227, 1977.

1252 [Ristovski, Z. D., Suni, T., Kulmala, M., Boy, M., Meyer, N. K., Duplissy, J., Turnipseed, A.,](#)
1253 [Morawska, L., and Baltensperger, U.: The role of sulphates and organic vapours in](#)
1254 [growth of newly formed particles in a eucalypt forest, Atmos. Chem. Phys., 10, 2919-](#)
1255 [2926, 10.5194/acp-10-2919-2010, 2010.](#)

1256 Rudels, B., Björk, G., Nilsson, J., Winsor, P., Lake, I., and Nohr, C.: The interaction between
1257 waters from the Arctic Ocean and the Nordic Seas north of Fram Strait and along the

1258 East Greenland Current: results from the Arctic Ocean-02 Oden expedition, *Journal of*
1259 *Marine Systems*, 55, 1-30, 2005.

1260 Schmidtko, S., Johnson, G. C., and Lyman, J. M.: MIMOC: A global monthly isopycnal
1261 upper-ocean climatology with mixed layers, *Journal of Geophysical Research:*
1262 *Oceans*, 118, 1658-1672, 10.1002/jgrc.20122, 2013.

1263 Schoemann, V., Becquevort, S., Stefels, J., Rousseau, V., and Lancelot, C.: Phaeocystis
1264 blooms in the global ocean and their controlling mechanisms: a review, *Journal of Sea*
1265 *Research*, 53, 43-66, <http://dx.doi.org/10.1016/j.seares.2004.01.008>, 2005.

1266 Sharma, S., Chan, E., Ishizawa, M., Toom-Sauntry, D., Gong, S. L., Li, S. M., Tarasick, D.
1267 W., Leaitch, W. R., Norman, A., Quinn, P. K., Bates, T. S., Levasseur, M., Barrie, L.
1268 A., and Maenhaut, W.: Influence of transport and ocean ice extent on biogenic aerosol
1269 sulfur in the Arctic atmosphere, *J. Geophys. Res.*, 117, D12209,
1270 10.1029/2011JD017074, 2012.

1271 Simó, R.: Production of atmospheric sulfur by oceanic plankton: biogeochemical, ecological
1272 and evolutionary links, *Trends in Ecology & Evolution*, 16, 287-294, 2001.

1273 Stohl, A.: Computations, accuracy and applications of trajectories - A review and
1274 bibliography, *Atmos. Environ.*, 32, 947-966, 1998.

1275 Ström, J., Engvall, A.-C., Delbart, F., Krejci, R., and Treffeisen, R.: On small particles in the
1276 Arctic summer boundary layer: observations at two different heights near Ny-Ålesund,
1277 Svalbard, *Tellus B - Chemical and Physical Meteorology*, 61, 473-482, 2009.

1278 Suni, T., Kulmala, M., Hirsikko, A., Bergman, T., Laakso, L., Aalto, P. P., Leuning, R.,
1279 Cleugh, H., Zegelin, S., Hughes, D., van Gorsel, E., Kitchen, M., Vana, M., Hörrak,
1280 U., Mirme, S., Mirme, A., Sevanto, S., Twining, J., and Tardos, C.: Formation and
1281 characteristics of ions and charged aerosol particles in a native Australian Eucalypt
1282 forest, *Atmos. Chem. Phys.*, 8, 129-139, 10.5194/acp-8-129-2008, 2008.

1283 Tunved, P., Ström, J., and Krejci, R.: Arctic aerosol life cycle: linking aerosol size
1284 distributions observed between 2000 and 2010 with air mass transport and
1285 precipitation at Zeppelin station, Ny-Ålesund, Svalbard, *Atmos. Chem. Phys.*, 13,
1286 3643–3660, 10.5194/acpd-12-29967-2012, 2013.

1287 Warren, S. G., and Hahn, C. J.: Cloud climatology, in: *Encyclopedia of Atmospheric*
1288 *Sciences*, edited by: Holton, J. R., Pyle, J., and Curry, J. A., Academic Press, London,
1289 UK, 476-483, 2002.

rev. 2017-2-18 10:48

Formatiert: Nicht unterstrichen,
Rechtschreibung und Grammatik prüfen

1290 Wiedensohler, A., Covert, D., Swietlicki, E., Aalto, P., Heintzenberg, J., and Leck, C.:
1291 Occurrence of an ultrafine particle mode less than 20 nm in diameter in the marine
1292 boundary layer of the Arctic summer and autumn, *Tellus*, 48B, 213-222, 1996.

1293 Willis, M. D., Burkart, J., Thomas, J. L., Köllner, F., Schneider, J., Bozem, H., Hoor, P. M.,
1294 Aliabadi, A. A., Schulz, H., Herber, A. B., Leaitch, W. R., and Abbatt, J. P. D.:
1295 Growth of nucleation mode particles in the summertime Arctic: a case study, *Atmos.*
1296 *Chem. Phys. Discuss.*, 2016, 1-31, 10.5194/acp-2016-256, 2016.

1297 Zhang, M., Chen, L., Xu, G., Lin, Q., and Liang, M.: Linking Phytoplankton Activity in
1298 Polynyas and Sulfur Aerosols over Zhongshan Station, East Antarctica, *J. Atmos. Sci.*,
1299 72, 4629-4642, 2015.

1300
1301
1302

Parameter	TR (h)	Explanation
C25	1 min	25% percentile of cloud base from AWI ceilometer (m)
CF12, 24, 36, 48, 5D	24	Average MODIS cloud fraction during the last 12h, 24h, 36, 48h, and days 3-5 before trajectory arrival
D50	1	Number-median diameter of particles < 50 nm diameter
CS	1	Condensation sink (s^{-1})
DZ	1	Vertical trajectory displacement ($m h^{-1}$) during the last hour before arrival
MSA	≥ 1 day	Methane sulfonate ($nmol m^{-3}$)
N10	1	Number concentration of particles up to 10 nm ($>2010, cm^{-3}$)
N20	1	Number concentration between 10 and 20 nm (cm^{-3})
N25	1	Number concentration of particles up to 25 nm (cm^{-3})
N40	1	Number concentration between 20 and 40 nm (cm^{-3})
N60	1	Number concentration between 40 and 60 nm (cm^{-3})
N100	1	Number concentration between 60 and 100 nm (cm^{-3})
N300	1	Number concentration between 100 and 300 nm (cm^{-3})
Na	≥ 1 day	Sodium concentrations ($nmol m^{-3}$)
NCO	1	Number concentration of particles > 300 nm (cm^{-3})
nssSO ₄ ²⁻	≥ 1 day	Non-sea salt sulfate concentrations ($nmol m^{-3}$)
NTO	1	Number concentration of particles ≥ 10 nm, (cm^{-3})
OC12, 24, 36, 48, 5D	120	Average MODIS DMSPt (nmol) during the last 12h, 24h, 36, 48h, and days 3-5 before trajectory arrival
OW12, 24, 36, 48, 5D	24	Average open water (%) during the last 12h, 24h, 36, 48h, and days 3-5 before trajectory arrival
PRE	1	Trajectory precipitation (mm) at arrival
RH	1	Trajectory relative humidity (%) at arrival
SFL	1	Solar flux at trajectory arrival ($W m^{-2}$)
SP12, 24, 36, 48, 5D	1	Accumulated precipitation (mm) during the last 12h, 24h, 36, 48h, and days 3-5 before trajectory arrival
T12, 24, 36, 48, 5D	24	Average sea surface temperature (C) during the last 12h, 24h, 36, 48h, and days 3-5 before trajectory arrival
TEM	1	Trajectory temperature (C) at arrival
WDR	1	Trajectory wind direction ($^{\circ}$) during the last hour before arrival
WSP	1	Trajectory wind speed ($m sec^{-1}$) during the last hour before arrival

1304

1305

Table 1 Aerosol, atmospheric, and ocean parameters utilized in the present study.

1306

DMSPt = Total dimethylsulfoniopropionate in surface ocean waters. TR = temporal

1307

resolution in which the respective data were available. [All parameter explanations](#)

1308

[starting with "Trajectory" refer to parameters calculated by HYSPLIT4 at each](#)

1309

[trajectory step.](#)

1310

1311
 1312
 1313
 1314
 1315
 1316
 1317
 1318

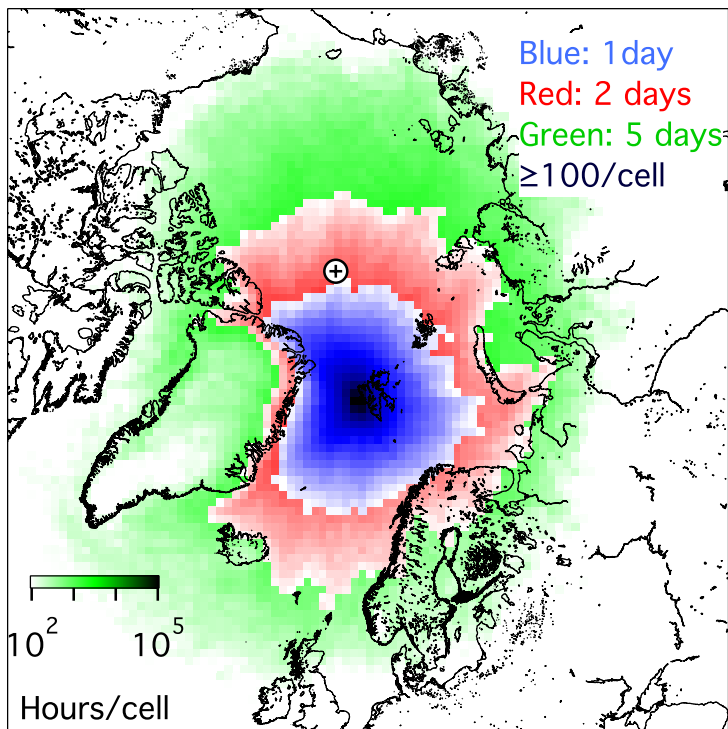
Approach	Acronym	Criteria and thresholds	Total number of events	Number of unique events	<u>% of total number of data hours</u>
Percentiles	PCT	N25 >93%-percentile	4143	240	<u>1</u>
Diameter-growth	DGR	D50-Growth >1.5	1199	235	<u>3</u>
Multi-size growth	MEV	Multi-growth >1.6	1191	266	<u>4</u>
Sum			6533	741	

rev. 2017-2-18 10:48
 Formatierte Tabelle
 rev. 2017-2-18 10:48
 Eingefügte Zellen

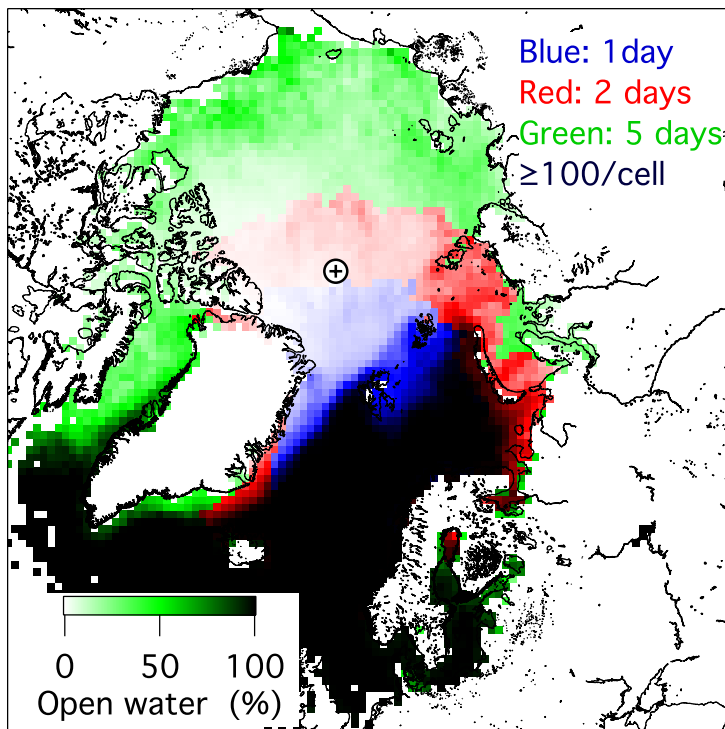
1319
 1320
 1321
 1322
 1323

Table 2 Total and unique number of events of new particle formation identified by the three approaches to identify NPF-events, and percent of all data hours covered by unique events.

rev. 2017-2-18 10:48
 Gelöscht: .



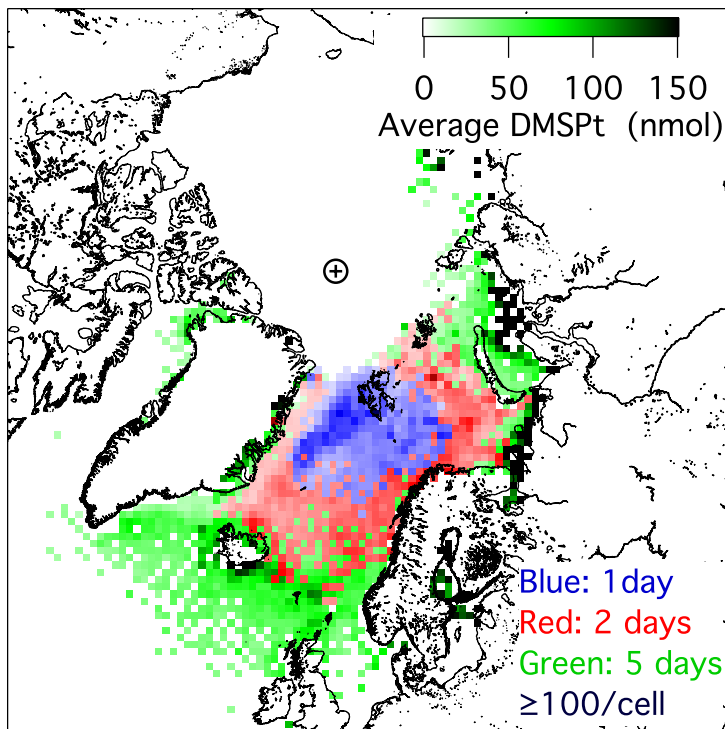
1325
 1326 Fig. 1 Map of the regional distribution of 5-day (green), 2-day (red), and 1-day (blue)
 1327 hourly back trajectories to Mt. Zeppelin during the months March through October
 1328 of the years 2006 - 2015. Black symbol: North Pole. The colored areas are covered
 1329 with at least 100 trajectory hours per geocell and the color saturation corresponds to
 1330 the number of trajectory hours per grid cell on a log-scale.
 1331



1332

1333 Fig. 2 Map of the regional distribution of open water under 87648 5-day (green), 2-day
 1334 (red), and 1-day (blue) hourly back trajectories to Mt. Zeppelin during the during the
 1335 months March through October of the years 2006-2015. Black symbol: North Pole.
 1336 The areas are covered with at least 100 trajectory hours concurrent with data values
 1337 per geocell.

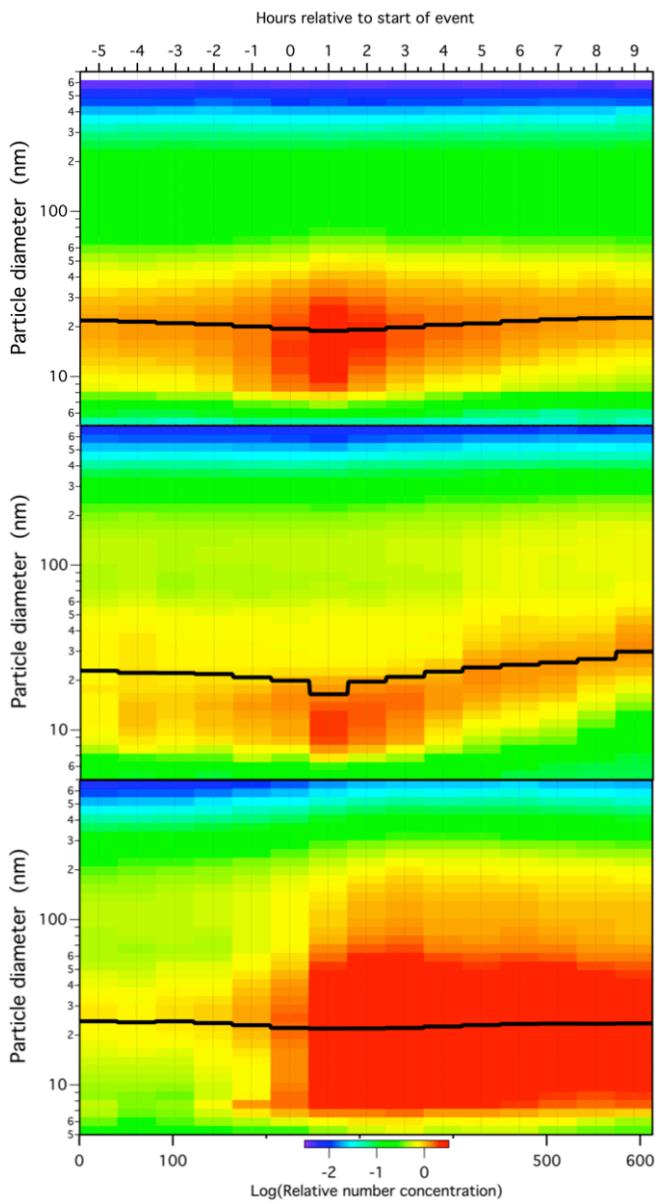
1338



1339

1340 Fig. 3 Map of the regional distribution of DMSPt along 87648 5-day (green), 2-day (red),
 1341 and 1-day (blue) hourly back trajectories to Mt. Zeppelin during the during the
 1342 months March through October of the years 2006-2015. Black symbol: North Pole.
 1343 The relative color scale holds for all colors. The areas are covered with at least 100
 1344 trajectory hours with data values per geocell.

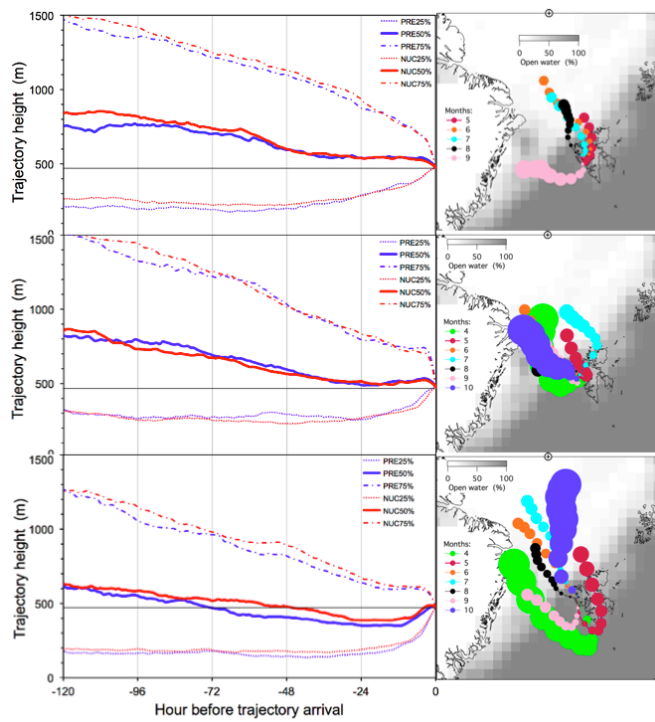
1345



1346

1347 Fig.4 Average temporal development of the relative number size distribution before and
 1348 during NPF-events identified by the three approaches. The black curve gives the
 1349 median sub-50-nm particle diameter D50 during the events. Top: PCT-events;
 1350 center: DGR-events; bottom: MEV-events.

1351

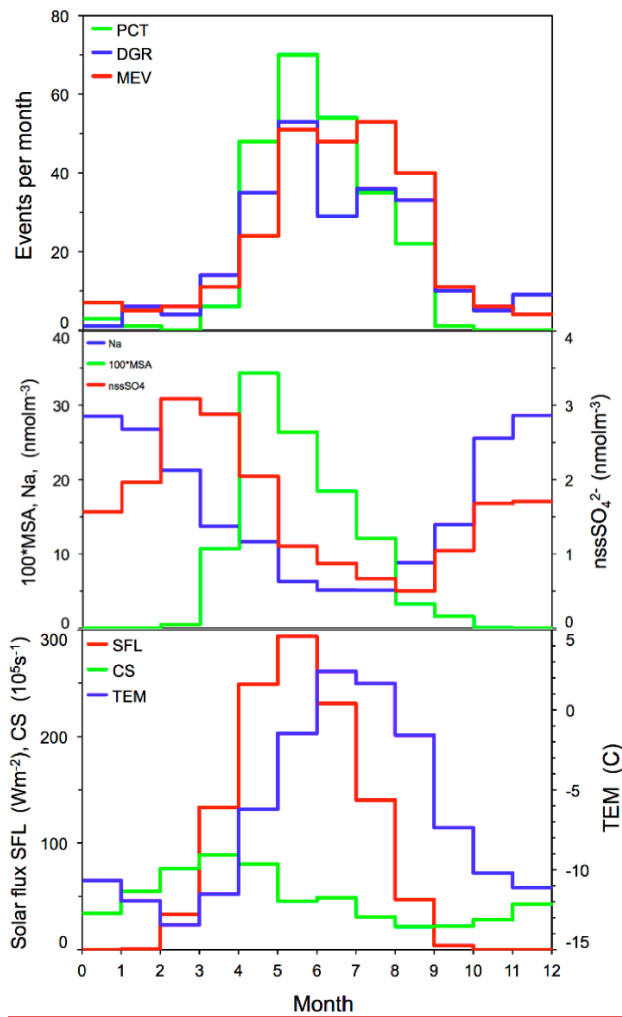


1352

1353 Fig. 5 Left panels: Median back trajectory height profiles (m) during the six pre-event
 1354 hours (full line in blue, PRENUC) and during the nine DGR-event hours (full line in
 1355 red, NUC). 25% and 75% percentiles are shown as dotted, and dash-dotted lines,
 1356 respectively. Top: PCT-events; center: DGR-events; bottom: MEV-events. The thin
 1357 horizontal line marks the station level.

1358 Right panels: Average monthly trajectory positions in 12 h steps for the months April
 1359 through October. Only months with at least 10 NPF-events are shown. The circles
 1360 comprise 95% of all trajectories at any trajectory step. The underlying grey-scale
 1361 map indicates July ice cover averaged over the years 2006 – 2015

1362



1363

1364 Fig. 6 Top: Monthly numbers of new particle formation events according to the three

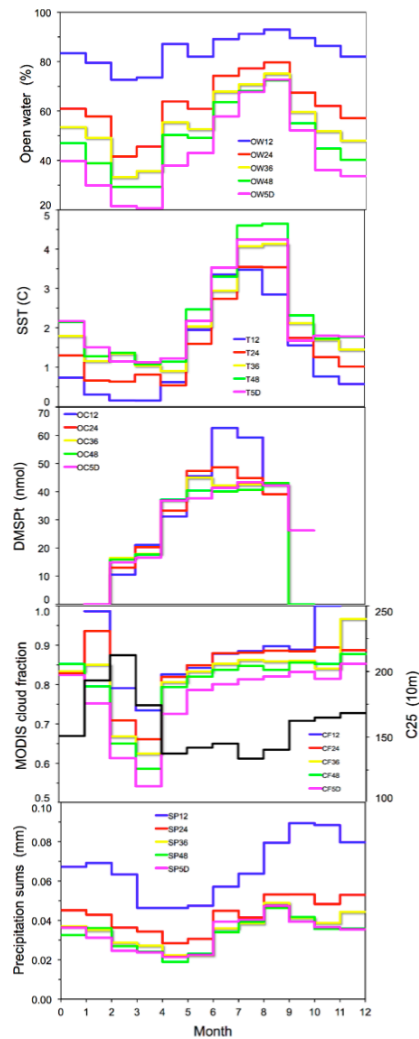
1365 approaches, summed up over the whole period of ten years, PCT: Upper percentile
 1366 of N25; DGR: Diameter growth; MEV: Multiple size events.

1367 Center: Average seasonal distribution of particle composition in nmolm^{-3} .
 1368 Na = sodium, nssSO_4^{2-} = nssSO_4^{2-} , MSA = Methane sulfonate times 100.

1369 Bottom: Monthly average solar flux (SFL, red, Wm^{-2}), and temperature (TEM, blue
 1370 $^{\circ}\text{C}$), and condensation sink, (CS, 10^5s^{-1}), at Mt. Zeppelin, Spitsbergen.

1371

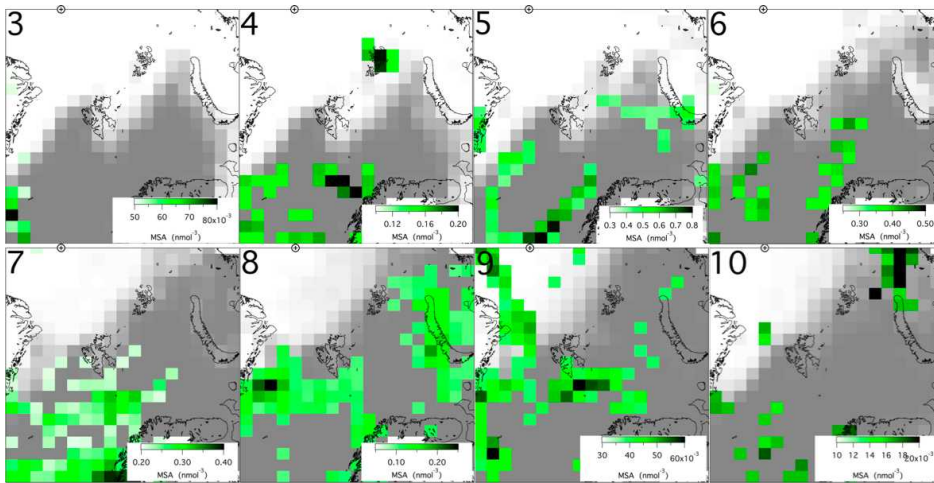
rev. 2017-2-18 10:48
 Gelöscht: .



1374

1375 Fig. 7 Monthly averages of environmental parameters averaged along back trajectories to
 1376 Mt. Zeppelin. From top to bottom: OW12-5D: Open water in % during last 12, 24,
 1377 36, and 48h, and days 3-5 before trajectory arrival at Mt. Zeppelin. T12-5D: Same
 1378 for sea surface temperature in °C. OC12-5D: Same for DMSPt in nmol in surface
 1379 waters. CF12-5D: Same for MODIS cloud fraction. SP12-5D: Same for
 1380 precipitation sums in mm. C25 = 25%-percentile of cloud base in decameter.

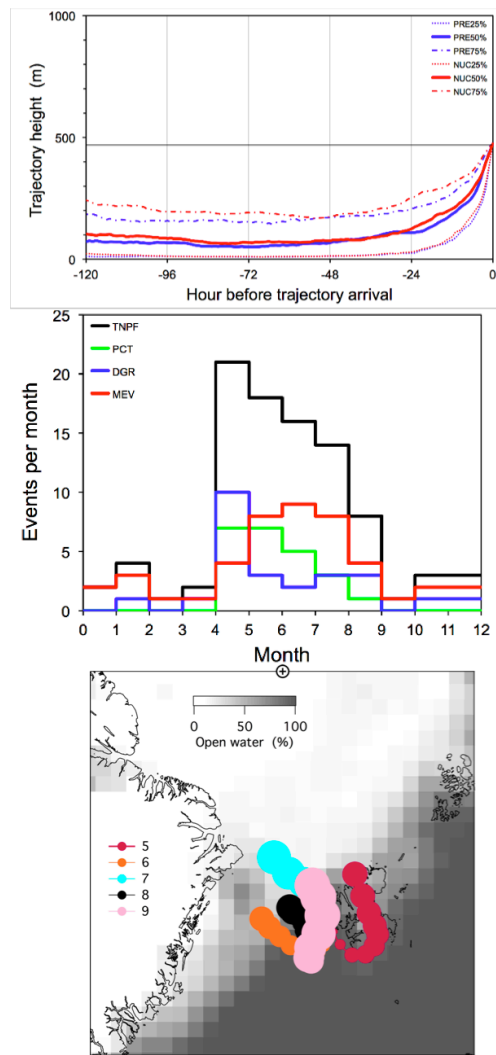
1381



1382

1383 Fig. 8 Average monthly distribution of methane sulfonic acid, (MSA, nmolm^{-3}), during the
 1384 months March–October of the years 2006–2015, constructed from MSA-
 1385 concentrations measured on Mt. Zeppelin, which were extrapolated along 5-day back
 1386 trajectories. Average open water percentages during the respective months are
 1387 indicated as white (0% open water) to dark grey (100% open water) areas. The
 1388 position of the North Pole is marked as cross in circle on the upper border of the
 1389 maps.

1390

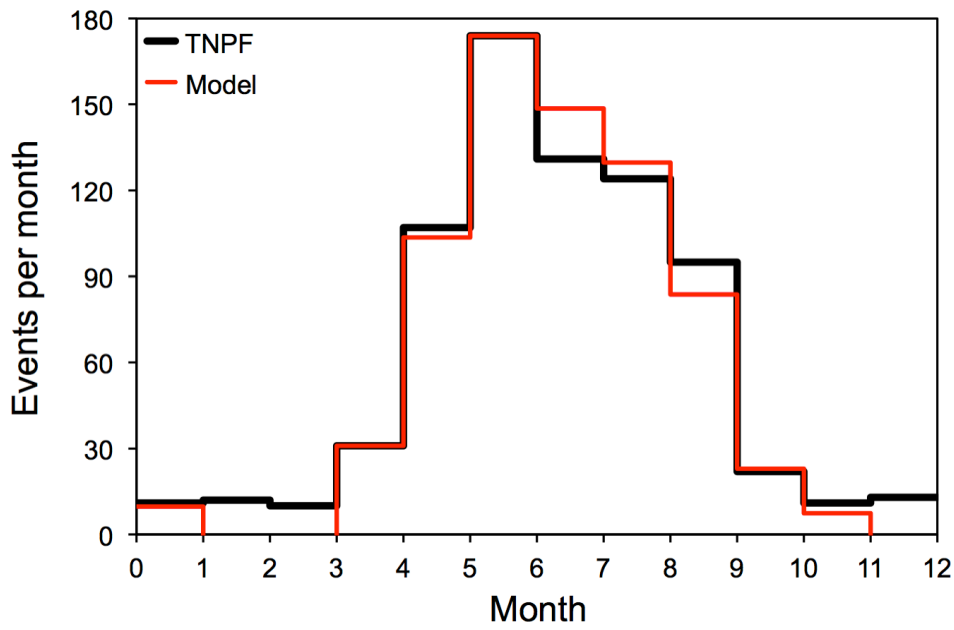


1391

1392 Fig. 9 Characteristics of the subpopulation of 93 NPF-events with back trajectories that
 1393 stayed below 500 m for five days before arrival. Top: Statistics of related vertical
 1394 trajectory coordinates as in Fig. 5. Center: Average monthly occurrence of PCT,
 1395 DGR, and MEV-events, summed up over the whole period of ten years. Bottom:
 1396 Related average monthly trajectory positions in 12 h steps for the months May
 1397 through September. The circles comprise 95% of all trajectories at any trajectory

rev. 2017-2-18 10:48
 Gelöscht: .

1399 step. The underlying grey-scale map indicates July ice cover averaged over 2006 –
1400 2015.
1401

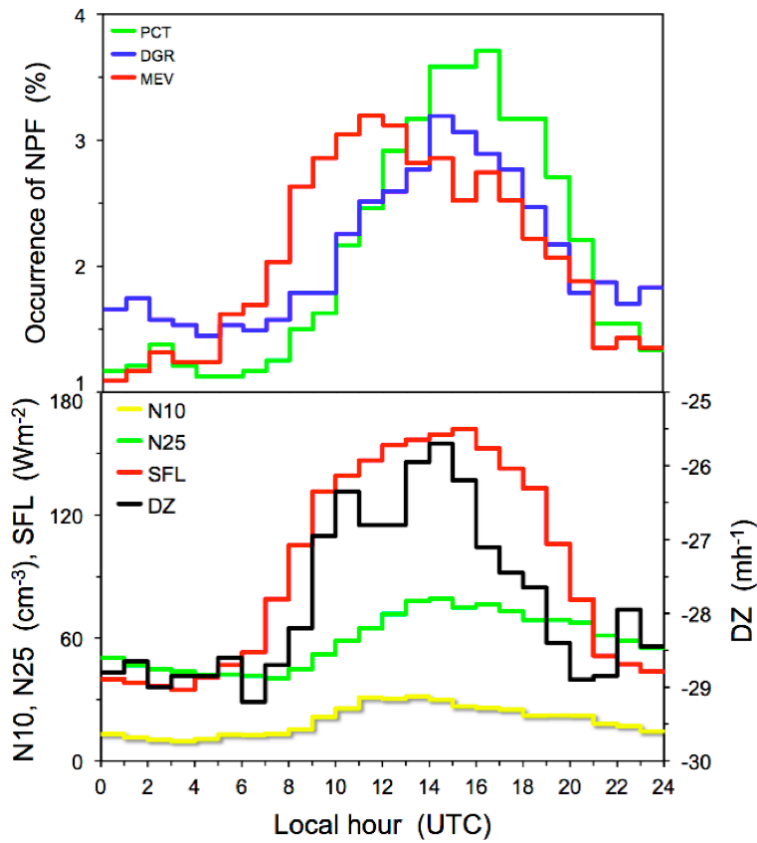


1402

1403 Fig. 10 Average monthly sums of NPF-events due to the three types of new particle
 1404 formation, (TNPF, black), summed up over the whole period of ten years, Red:
 1405 Three-parameter model to describe TNPF.

1406

rev. 2017-2-18 10:48
 Gelöscht:)



1408

1409 Fig. 11 Top: Relative average diurnal occurrence of the three types NPF-events. PCT:
 1410 Upper percentile of N25; DGR: Diameter growth; MEV: Multiple size events.
 1411 Bottom: Average diurnal variation of the HYSPLIT-modeled solar flux (SFL, Wm⁻²),
 1412 the integral particle concentrations N10, and N25 in cm⁻³, and of the vertical
 1413 displacement parameter (DZ, mh⁻¹). N10 is based on data of the years 2011 – 2015
 1414 whereas the other parameters are based on data of the years 2006 – 2015.